



8-2015

## Low Melting Glass Frit as an Adhesion and Resistivity Promotor to Silver Nanoparticle Ink Photonically Sintered on Indium Tin Oxide Coated Glass

Jason J. Kleiner  
*Western Michigan University*

Follow this and additional works at: [https://scholarworks.wmich.edu/masters\\_theses](https://scholarworks.wmich.edu/masters_theses)

 Part of the Chemical Engineering Commons

---

### Recommended Citation

Kleiner, Jason J., "Low Melting Glass Frit as an Adhesion and Resistivity Promotor to Silver Nanoparticle Ink Photonically Sintered on Indium Tin Oxide Coated Glass" (2015). *Masters Theses*. 625.  
[https://scholarworks.wmich.edu/masters\\_theses/625](https://scholarworks.wmich.edu/masters_theses/625)

This Masters Thesis-Open Access is brought to you for free and open access by the Graduate College at ScholarWorks at WMU. It has been accepted for inclusion in Masters Theses by an authorized administrator of ScholarWorks at WMU. For more information, please contact [wmu-scholarworks@wmich.edu](mailto:wmu-scholarworks@wmich.edu).



LOW MELTING GLASS FRIT AS AN ADHESION AND RESISTIVITY PROMOTOR  
TO SILVER NANOPARTICLE INK PHOTONICALLY SINTERED ON INDIUM TIN  
OXIDE COATED GLASS

by

Jason Kleiner

A thesis submitted to the Graduate College  
in partial fulfillment of the requirements  
for the Masters of Science in Engineering  
Chemical Engineering  
Western Michigan University  
August 2015

Thesis Committee:

Margaret Joyce, Ph.D., Chair  
Thomas Joyce, Ph.D.  
Raja Aravamuthan, Ph.D.

# LOW MELTING GLASS FRIT AS AN ADHESION AND RESISTIVITY PROMOTOR TO SILVER NANOPARTICLE INK PHOTONICALLY SINTERED ON INDIUM TIN OXIDE COATED GLASS

Jason Kleiner, M.S.E.

Western Michigan University, 2015

The objective of this study was the fabrication of a printed circuit resulting from the photonic drying/sintering of conductive circuits, printed using silver nano ink layered on a film of low melting glass frit onto indium tin oxide (ITO) coated glass substrate through the flexographic printing method. The fabrication process flow included material preparation, printing, and photonic drying/sintering in that order.

Investigation of the breakthrough photonic drying/sintering method was studied by varying sintering parameters, specifically the amount of heat energy applied to each specimen, and the speed at which it was applied. Additionally, the adhesion promoting properties of a never before studied glass frit was investigated. Their effects were studied by quantifying adhesion and resistivity of the printed film. Adhesion was quantified by mechanically applying abrasive forces, and resistance was measured through the use of a four point collinear probe.

Adhesion improved with an increase in energy flux, and presence of frit, for which both factors were statistically significant. Adhesion decreases with increase in sintering speed. Resistivity decreases dramatically for an increase in energy flux applied and presences of the adhesion promoter has no significant effect. A clear trend for resistivity as a function of sintering speed could not be observed.

Copyright by  
Jason Kleiner  
2015

## ACKNOWLEDGEMENTS

I would like to thank my committee, Dr. Margaret Joyce, Dr. Thomas Joyce, and Dr. Raja Aravamuthan. They were always available to advise and to offer guidance, whether it related to the research or not.

Thanks goes to Michael Joyce, Matthew Stoops, Dan Fleming, Sai Avuthu, Sepehr Emamian, and Ali Eshkeiti for assistance with troubleshooting and understanding of the lab equipment and lab techniques.

Special thanks goes to Gentex Corp. and Hitachi Ltd for providing materials.

Most of all I would like to thank and acknowledge my wife, Alexa. Whom none of this would be possible without her encouraging, and supporting me through this endeavor.

Jason Kleiner

## TABLE OF CONTENTS

ACKNOWLEDGEMENTS .....	ii
LIST OF FIGURES .....	v
LIST OF TABLES .....	viii
CHAPTER	
I. INTRODUCTION .....	1
II. LITERATURE REVIEW.....	3
Process & Critical Process Parameters .....	3
Material Preparation.....	3
Printing Process .....	4
Ink .....	5
Adhesion Promoter .....	10
Substrate .....	12
Printing Method .....	13
Drying and Sintering.....	14
Quality Testing .....	20
Adhesion .....	21
Resistivity .....	23
III. EXPERIMENTAL METHODS .....	25
Design of Experiment .....	25
Surface Preparation.....	27

## Table of Contents - Continued

CHAPTER	
Printing.....	28
Photonic Curing.....	31
Adhesion Testing.....	33
Resistivity.....	41
IV. RESULTS.....	42
Adhesion .....	45
Resistivity.....	51
V. CONCLUSIONS .....	57
VI. RECOMMENDATIONS FOR FURTHER STUDY .....	58
REFERENCES.....	60
APPENDIX.....	65

## LIST OF FIGURES

1. Process Flow for Fabrication and Qualification of Printed Conductive Film .....	3
2. Melting Point Temperature of Gold Nanoparticles as a Function of Particle Size [9]. ...	8
3. Annealing of Silver Metal Film (a) without glass frit, and (b) with glass frit at 600°C [12]. .....	11
4. Hitachi Low Melting Glass Softening Characteristics [13]. .....	12
5. Schematic of Flexographic Printing Method .....	14
6. Resistivity of Photonicallly Cured 2.5 $\mu\text{m}$ Thick Nano Silver Ink Film on Mylar [10].	19
7. Densification of a 35 $\mu\text{m}$ Silver Nanoparticle Film on Glass. [15] .....	20
8. Contact Angle of Ink Droplet on Substrate [2]. .....	22
9. Keithley Four Point Probe for Measuring Resistivity. [22] .....	25
10. Design of Experiment .....	26
11. Scanning Electron Microscope Images of VS1307 at Different Magnification, Courtesy of Western Michigan University Chemistry Department. ....	28
12. Harper Scientific Carriage Assembly with Non-Image Rubber Transfer Roll .....	30
13. Classification of Adhesion Results [30]. .....	36
14. Abrasion Action Utilized by Taber 5130 [31]. .....	37
15. Sample Diagram of Taber Test Specimen .....	39



## List of Figures - Continued

16. ImageXperts Analysis: Determining Glass from Printed Film. ....	40
17. Comparison of Specimens Post Abrasion Analyzed by Image Expert Software for Percent Glass Exposed.....	41
18. Schematic for Average Resistivity Measurement .....	42
19. Scanning Electron Microscope image of (a) without VS1307 and (b) with VS1307. ....	43
20. Normal Probability Plots for Percent Film Remaining and Resistivity for Experiment 1 and 2.....	44
21. Multiple Experiment Comparison of Percent Film Remaining .....	45
22. Comparison of Percentage of Film Remaining on Substrate for Changes in Energy, With/Without Frit. ....	46
23. Main Effect Plot for Percent Film Remaining on Substrate for Experiment 1.....	47
24.A) Pareto Chart and B) Normal Plot of the Standard Effects for Percent Film Remaining for Experiment 1.....	48
25. Comparison of Percent of Film Remaining at Different Print Speeds Without/With Frit. ....	49
26. Main Effect Plot for Percent Film Remaining on Substrate for Experiment 2.....	50
27.A) Pareto Chart and B) Normal Plot of the Standard Effects for Percent Film Remaining for Experiment 2.....	50
28. Comparison of Sheet Resistance for Different Energy, With and Without Frit.....	52
29. Main Effect Plot of Film Resistance for Experiment 1.....	53
30.A) Pareto Chart and B) Normal Plot of the Standard Effects on Film Resistance for Experiment 1. ....	53
31. Comparison of Film Sheet Resistance for Different Sintering Speeds, With and Without Frit.....	54
32. Main Effect Plot of Film Resistance for Experiment 2.....	55

## List of Figures - Continued

33.A) Pareto Chart and B) Normal Plot of the Standard Effects on Film Resistance for Experiment 2. ....	55
34. Interaction Plot of Sintering Speed and Adhesion Promoting Frit for Film Resistivity.....	56

## LIST OF TABLES

1. Resistivity of Common Conductors in Printed Electronics [6] [7]. .....	6
2. Metal Nanoparticle and Surfactants Used in Industrial Conductive Ink [2]......	9
3. Sintering Profiles for Novacentrix PulseForge 1200 Used for Proof of Concept. ....	33
4. Comparison of Tapes Used for ASTM D3359 [29]. .....	34

## CHAPTER I

### INTRODUCTION

An emerging \$300 billion market is expected to be nurtured through the combination of microelectronics, chemistry, and printing, to form an industry known as printed electronics (PE). Industrial and consumer applications are expected in the automotive, building and architecture, chemical, medical, consumer electronics, packaging, and energy industries. [1]

The benefits of PE are realized in both industrial products and processes. The breakthroughs within PE will create thin, light weight, potentially wearable electronics that could not previously be achieved. PE will eventually offer manufactures a means to cost-effectively mass produce products at affordable prices by reducing production and material costs. Silicon technology has reached its ultimate fine pitch resolution of 13 nm, where pitch refers to the spacing between pixels or unique formations that have been printed. Huge investment is needed to establish a production facility to achieve an ultimate fine pitch of 13 nm. PE requires one-tenth to one-one hundredth of the investment as for an equivalent silicon based manufacturing facility [2].

Applications of PE, such as printed wiring boards have been around since the 1950's, but PE did not emerge as the ultimate solution [2]. Complications result from the PE printing process that effect product quality. One example is the large footprint and long cycle time

needed to densify conductive metallic nanoparticles contained in the PE inks with conventional curing ovens [1]. Densification, or reducing the occupied volume given a particular mass of metallic nanoparticles contained within the ink, allows for an increase in conductivity. Conductivity increases as a result of increased surface area contact. Breakthroughs for this concern include recently developed methods of densification through the use of photonic sintering. One additional concern is the adhesion of printed circuit inks on exceptionally smooth surfaces, such as glass. Breakthrough adhesion promoters, such as materials with like chemistries similar to the substrate, may be the answer. No research has been performed on the marriage of these countermeasures to the aforementioned concerns.

The objective of this study was the fabrication of a printed circuit resulting from the photonic sintering of conductive circuits, printed using silver nano ink layered on a film of low melting glass frit onto ITO coated glass substrate through the flexographic printing method. In addition to fabrication of the aforementioned circuit, an investigation of the relative adhesion and resistivity was conducted. Adhesion was quantified by an abrasion test and resistance was measured through the use of a four point collinear probe.

## CHAPTER II

### LITERATURE REVIEW

#### Process & Critical Process Parameters

The fabrication and qualification process is comprised of 1) material preparation, 2) printing 3) photonic curing (a.k.a. sintering), and 4) two types of quality tests. Figure 1 illustrates the process flow from beginning to end. An in depth literature review on each process step will now be provided.



Figure 1. Process Flow for Fabrication and Qualification of Printed Conductive Film.

#### Material Preparation

Cleaning is essential and a common step performed when attempting to print on coated glass. This becomes evident in chapter 0, a look at the impacts to adhesion before the

sintering process step. A common method of cleaning glass in an industrial setting is a three consecutive bath system, consisting of trichloroethylene, acetone, and isopropyl alcohol in that order. This sequential cleaning has been used successfully by the electronics industry for many years [3].

Trichloroethylene (TCE) is a halogenated alkene, and has been long recognized by a number of different industries for its cleaning power. TCE is a dense substance (1.46 kg/L) with a high vapor density that allows for relatively easy recovery from vapor degreasing systems. It dissolves soils faster, resulting in a cleaner substrate, and provides high output of cleaned glass per unit time [4]. TCE leaves a trace residue when dried, therefore acetone is used to clean further. Similarly to TCE, the acetone also leaves a residue, and, likewise, isopropyl alcohol is used to remove the trace acetone. Isopropyl alcohol, with its low vapor pressure will evaporates leaving no trace on the glass.

### Printing Process

Printing is a multifaceted process from which raw materials are such as ink, and substrate undergo physical changes in order to produce the end product, and can be done with a variety of different printing methods. Depending on the nature of the PE product, considerations for ink and specialized additives to the ink, substrate and print method must be taken.

## Ink

The choice of ink is important to any printing process. For example, archival ink is chosen for its resistance to fade over a long period of time to aid in document preservation. Another example is related to decorative processes such as artistic and aesthetic appeal; acrylic ink is used for its fast curing properties in that application. For the PE industry, nano silver inks are chosen for their electrical conductivity, low sintering temperature, resistance to oxidation, and cost [2].

Conductivity is the measure of how easily a material can allow electrons to flow. Drude first proposed the model for conduction leading to the famous Ohm's law in 1900. Drude's model considers an array of atoms plus a collection of free electrons. When an electric field is applied, the free electrons drift slowly in a direction opposite to that of the electric field [5]. This is what is known as current, and materials having a greater number of free electrons, known as conductors, will produce a greater current for a given electric field. Because an electrical field can be varied, it is common-place to categorize different conductors by keeping the electric field constant (thus a constant electrical potential) and measuring the current produced by each conductor. Then, through the use of Ohm's law presented in Equation 1, the resistances of each conductor can be directly compared.



$$R = \frac{E}{I}$$

Equation 1

Where R is resistance (Ohms,  $\Omega$ )

I is current (Amps)

E is magnitude of electrical potential (Volts)

The conductors used in printed electronics are usually silver, copper, or gold.

Table 1 shows the resistivity of each material. The values are corrected for thermal expansion, and are taken from annealed 99.999% or purer bulk metal at 25°C .

Table 1. Resistivity of Common Conductors in Printed Electronics [6] [7].

Element	Resistivity (20 °C) ( $10^{-8} \Omega \text{ m}$ )	Price (USD/Troy oz)
Silver	1.59	15
Copper	1.68	0.20
Gold	2.21	1105

Resistance to oxidation is a major consideration of ink compatibility. Oxidation states of particular metals can decrease conductivity, and introduce other detrimental

characteristics such as brittleness and a loss in adhesion. Pure copper can oxidize over time and exposure to other substances to form a variety of compounds, usually with oxidation states +1 and +2, commonly referred to as cuprous and cupric respectively [8]. These compounds, such as cupric carbonate and cupric sulfate have the aforementioned undesirable properties. Metals such as silver and gold also have oxidation states, but unlike copper, silver and gold does not oxidize in the presence of air alone [9]. Another benefit offered by silver and gold is the conductivity of the oxidized silver and gold is only slightly reduced. For this reason, silver and gold are used where conductivity cannot be a compromised quality of the end product [10].

As with all manufacturing processes, cost is another key aspect of metal selection. From Table 1 it can be seen that, as of July 2015, the price of copper is 20 cents /troy oz, silver is \$20 / troy oz, and gold is \$1250 /troy oz [7]. Many manufactures consider the cost advantages of copper outweigh the relatively higher resistivity and the fact that it will oxidize with air over time.

The conducting metal particles typically found in conductive ink can come in a variety of sizes ranging from micro to nanometer sized particles. There is a change in physical properties of the metal that comes with the geometric changes in the metal. Nanoparticles have high surface area to mass ratio, high absorptivity, poor thermal conductivity, and low thermal mass. These properties depress the sintering temperature of the metal [11]. Figure 2 illustrates this phenomenon with the melting point depression of gold nanoparticles with respect to size. As shown, the melting temperate increases as the nanoparticles become larger. This is true for all metallic particles at the nanoscale.

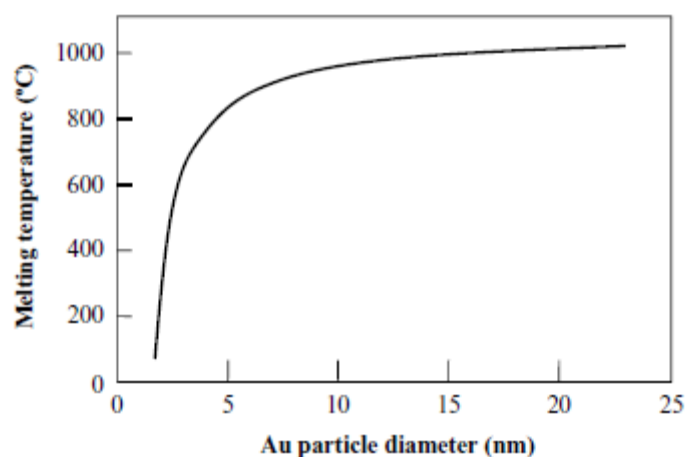


Figure 2. Melting Point Temperature of Gold Nanoparticles as a Function of Particle Size

[11]

This melting point depression allows for a densification of metal particles after sintering, ultimately increasing the conductivity of the ink in the printed circuit.

Nanoparticles can be made through a number of different processes, including the reduction of organometallic compounds in solution, mechanical means such as laser abrasion or vapor processes in which bulk metals are evaporated and condensed [2]. The work of Schroder (2006) describes this vapor nanoparticle synthesis process in which a high power arc discharge (50-100 kA) is drawn between the rods of the desired metal nano particle in atmospheric pressure gas. The material at the end of the rod is ablated and heated to form a high pressure metal plasma. The plasma expands and is quenched by the surrounding gaseous atmosphere. The quenching yields nanometer sized, single

crystal, aggregated particles in a gas suspension. These particles are then collected and further treated depending on the application [12].

To keep the nanoparticles from agglomerating, surfactants are used. Table 2 shows different surfactants for gold, silver, and copper nanoparticles.

Table 2. Metal Nanoparticle and Surfactants Used in Industrial Conductive Ink [2].

Metal Nanoparticle	Surfactants
Au	Dodecanethiol
	Triphenylphosphine
	Polyvinylpyrrolidone (PVP)
	Polyethylene glycol (PEG)
Ag	Dodecanamine
	Phthalocyanine
	Polyvinylpyrrolidone (PVP)
	Polyethylene glycol (PEG)
Cu	Polyvinylpyrrolidone (PVP)
	Polyethylene glycol (PEG)

Polymeric surfactants increase adhesion of ink to the substrate during the sintering process, due to the strong networks of particles that are formed [2].

The metal is only part of the mixture that constitutes the ink as a whole; another constituent is the binder. The binder, as the name suggests, binds the metallic particles into a semisolid substance, giving the particles adhesion and cohesion. Otherwise the

particles could not be used with any printing method. Binders can be made of many different substances depending on the desired properties. For example, a water-based binder would be used when cleaning and environmental contamination are an issue, or for medical and packaging applications where residual solvent could be an issue [13].

### Adhesion Promoter

Adhesion promoters are substances in contact with the ink for the purpose of increasing the adhesive and cohesive forces between the ink and substrate. Adhesion promoters need not utilize both types of forces, but should increase the overall adhesion.

The work of Jang, et al. (2008) describes microstructural evolutions during the annealing process of silver nano ink with and without glass frit applied to a glass substrate by means of ink-jet printing, and annealed at high temperatures ( $> 400^{\circ}\text{C}$ ). The microstructural evolutions were considerably different for films with and without nanometer sized glass frit. These differences can be seen in Figure 3.a-b. Figure 3.a shows poor adhesion between the silver film and glass substrate, as seen by the presence of pores and voids between silver particles. Figure 3.b shows the filling of these pores and voids in the film by glass. The addition of the glass frit was shown to be beneficial to the overall adhesion of the film by way of grain growth. Grain growth is defined as the process of initially small grains melting together to form larger grains of silver and glass frit. Microstructural features found on at the level of the film clearly suggest that the glass frit melts to form a liquid phase when the annealing is performed above the glass

transition temperature. The liquid glass can effectively fill inter-granular pores between both silver nano particles and the glass substrate. The melting of the glass frit also induces a capillary stress that densifies the film via grain growth. The grains are readily rearranged in the presence of the liquid phase, accommodating large volumetric shrinkage and resulting in a crack-free, smooth, and dense film [12].

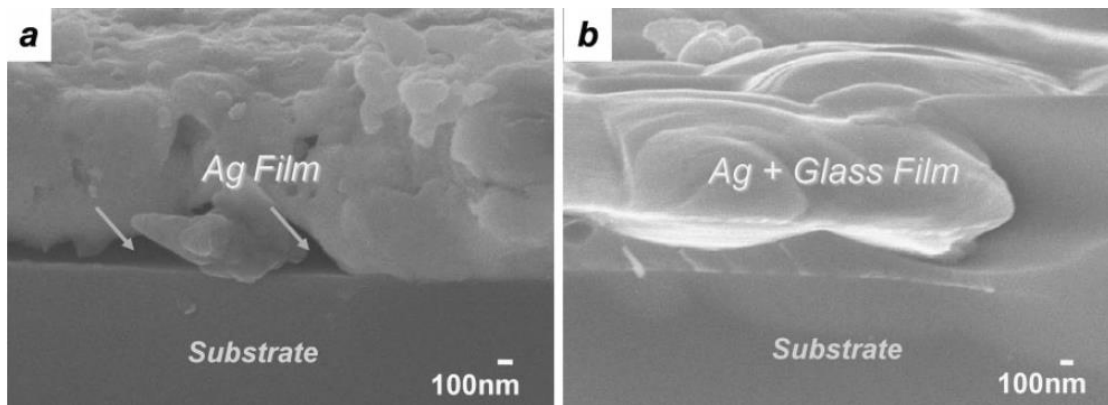


Figure 3. Annealing of Silver Metal Film (a) without glass frit, and (b) with glass frit at 600°C [14].

The addition of glass frit by Jang, et al. (2008) is an excellent example of increasing the mechanical forces between silver particle and substrate due to the geometry of both. The researches go on to test adhesion, using a standard according to American Society for Testing and Materials (ASTM D3359); a significant increase in adhesion for the specimens with a volume percentage of frit of 0.16 at 600 C was noted.

In 2012 Hitachi, Ltd. and Hitachi Chemical Co., Ltd. developed a low melting glass frit, able to melt in the range of 220 – 300 °C. Figure 4 illustrates the softening characteristics

of the low melting glass frit. By utilizing a proprietary technique to control the glass-network structure to allow the stable introduction of silver ions, a melting temperature reduces from a previous range of 350 – 400 °C to the aforementioned 220 – 300 °C range. This glass would act as the candidate for the adhesion promoter and is elaborated on in chapter 0 [15].

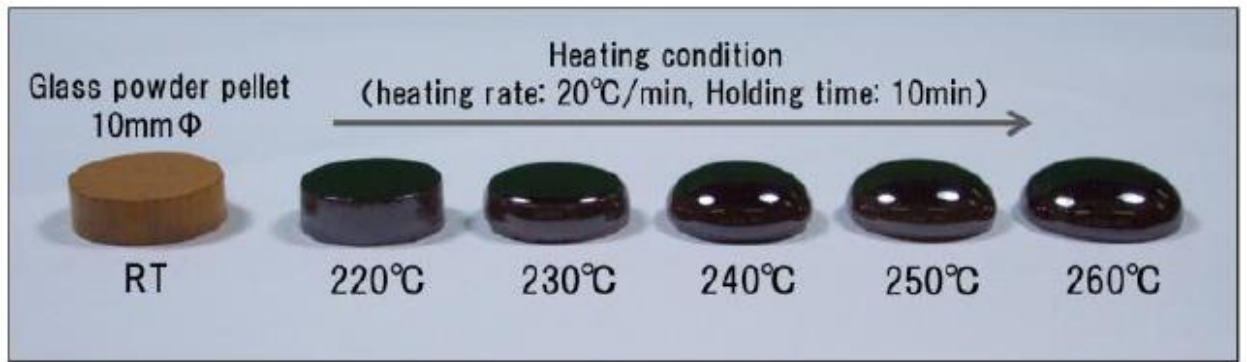


Figure 4. Hitachi Low Melting Glass Softening Characteristics [15].

#### Substrate

In addition to wetting control, a PE substrate is chosen for desirable characteristics such as optical transmittance, the ratio of the light falling on a body to that transmitted through said body. For example, a car's windscreen containing printed circuits must certainly provide adequate transmittance, so as not to hinder the driver. The combination of transparent substrates with transparent coatings is an aspect of the PE industry still under

much study. The coated substrate of interest is vapor deposited indium tin oxide (ITO) on glass. ITO is commonly used to pretreat glass prior to printing circuits on it.

ITO coated glass is an attractive, transparent electrode used widely for displays, photovoltaics, flat panel displays, lightings, electrochromic windows, and many other optoelectronic devices. Presently, ITO is commercially the most popular transparent conductor due to its low resistivity (approx.  $1 \times 10^{-4} \Omega \text{ cm}$ ) and high optical transmittance (85%) [16].

### Printing Method

Flexography (flexo) is a printing process currently used in many industrial applications. While screen printing dominates the PE industry today, flexo is used, Flexo accounts for less than 5% of industrial PE applications [17]. With speeds comparable to a rotary screen (500 m/min) print station, ease of scalability and a capability of producing line thicknesses of less than  $1 \mu\text{m}$ , flexo was a suitable candidate for study in this research.

Flexo is a relief process where the ink is deposited on the raised areas of a polymeric plate. This is in contrast to an intaglio, or engraving method, where the ink is deposited in the recessed cells of the plate or cylinder. Figure 5 is an illustration of the flexo process.

Flexo inks usually have a viscosity of 50-500 cP, and can be applied in a thickness as low as  $1 \mu\text{m}$  through the use of high resolution photo-polymeric plates. [2].



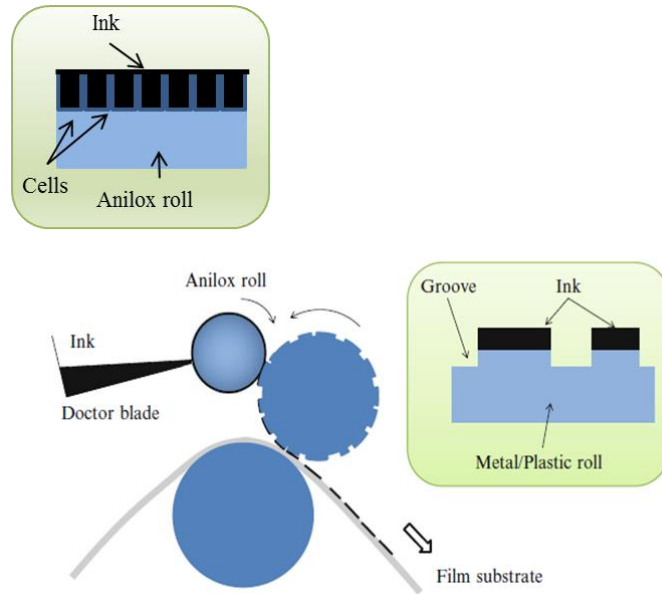


Figure 5. Schematic of Flexographic Printing Method

### Drying and Sintering

Drying is the process in which energy is added to the substrate/ink system in order to evaporate the solvent contained within the ink. Evaporation of the solvent allows for densification of the ink into a film, comprised from the ink's solids remaining on the substrate. These solids are electrically conductive, and what allows for the working circuit. If the energy applied during the drying step is sufficient enough that the particles will melt into a solid layer, sintering occurs. Sintering increases the area of contact and consequently increasing conductivity. The increase of conductivity is desirable when designing PE utilizing relatively small voltage potentials.

The bottle neck of any PE process is in the drying process. The drying step, necessary to render the precursor compounds conductive, typically requires more than 30 minutes and

elevated temperatures (250 ° C) for the metal contained in the ink to densify. If a web speed of 1 m/s is considered, the long sintering time makes roll to roll production very cost ineffective due to the necessary overall length of the line [1] [18]. Compensating with an increase in temperature can be unfeasible, as it introduces a condition in which the ink's solvent vaporizes or substrate deforms. Vaporization causes a “sputtering” effect, creating voids and discontinuity in the film, ultimately rendering defective product. Alternatively if the evaporation process is too slow, the ink may not densify, ultimately causing an increase in resistance. A balance in applied energy and time must be struck in any given sintering process, which often times leads to a bottle neck.

Additionally, the high temperatures needed for conventional sintering limits the types of substrates that can be used in printing. If the temperatures used are well below the melting temperatures of the bulk metal, the metal remains in the solid state. Considering that the metal nano particles are contained within the binder of the ink, only limited mass transfer along the substrate/ink interface is available for the metal nano particles. This results in a reduction of conductivity when compared to the bulk metal.

The metallization of silver nano ink by methods presented by Lee (2006) required a 30 min drying period in a 60° C oven and then post thermal treatment at 250° C for 30 min [19]. A breakthrough curing/sintering method was presented in K.A Schroder, et al. (2006).

The breakthrough sintering method, known as photonic sintering, offers the very specific advantage of rapidly heating the thin ink film created during the printing process while the remainder of the substrate remains cool. This is achieved by a broadcasted pulse of

high intensity light from a xenon bulb. Nano particles are usually thermally absorbing bodies of high surface area to mass ratio. As a result, little light is needed to heat the particles. With this system, heat is transferred to the ink film within milliseconds. The change-point for photonic vs conventional sintering is that photonic sintering emits an intense enough light that thermal equilibrium between particles and substrate is never achieved. The result is the particles are sintered, then cool before any substantial heat transfer to the substrate occurs. [12]

The model which explains the unique phenomena observed during photonic sintering is described by a one dimensional conduction equation. The heat conduction equation subject to time dependent heat flux boundary condition and volumetric source heating for the ink containing the metal nanoparticles is represented by Equation 2 [20].

$$\rho c_p \frac{\partial T}{\partial t} = \frac{\partial}{\partial x} \left( k \frac{\partial T}{\partial x} \right) + S$$

Equation 2

Where  $\rho$  is density of ink ( $\text{kg m}^{-3}$ )

$c_p$  is specific heat at constant pressure of ink ( $\text{J kg}^{-1} \text{K}^{-1}$ )

$k$  is thermal conductivity of ink ( $\text{W m}^{-1} \text{K}^{-1}$ )

$S$  is a volumetric source term ( $\text{m}^3$ )

$T$  is temperature (K)

$t$  is time (s)

Depending on the material, the heat pulse is treated as either a surface heat flux ( $\text{kW/cm}^{-1}$ ) or as a volumetric source term based on the absorptivity of the materials. If the heat pulse is treated as a surface flux, the boundary conditions at  $x=0$  and  $x=L$  are written, respectively as

$$q_0''(t) = q_p''(t) - h_{\infty,0}(T_0 - T_{\infty,0}) - \varepsilon\sigma T_0^4$$

Equation 3

$$q_L''(t) = h_{\infty,L}(T_L - T_{\infty,L})$$

Equation 4

Where  $q_p''(t)$  is the pulse waveform ( $\text{W m}^{-1}$ )

$\sigma$  is the Stefan-Boltzman constant ( $\text{W m}^{-2} \text{K}^{-4}$ )

$\varepsilon$  is the emissivity ( $q/q_{\text{black-body}}$ )

$h_{\infty,0}$  is the convective heat transfer coefficient ( $\text{W m}^{-1} \text{K}^{-1}$ )

$T_0$  is the surface temperature (K)

$T_{\infty,0}$  is the ambient surface temperature above the ink film. (K)

$L$  is the total depth of the material (m).

If the heat pulse is treated as a volumetric source term, then  $q_p''(t)$  is not included in Equation 3 and the incident heat pulse flux ( $q_0''$ ) is assumed to be absorbed volumetrically through the film stack according to Beer's law as

$$\frac{q''}{q_0''} = e^{-\alpha l}$$

Equation 5

Where  $q''$  is the heat flux transmitted through a planar volume of depth  $l$   
(kW cm<sup>-1</sup>)

$q_0''$  is the incident heat flux (W m<sup>-1</sup>)

$\alpha$  is the absorption coefficient (m<sup>-1</sup>)

The system comprised of the ITO coated glass, adhesion promoter layer, and silver nano ink layer is one whose heat pulse would be treated as a surface flux, due to the assumed small absorption coefficient of the coated glass [20] [21].

Several bodies of research have been published involving the photonic sintering of conductive nanoparticle ink onto substrate, including , Schroder (2006), Lee (2006), and West (2012) None of the publications addresses the adhesive properties of the silver nanoparticle film to the substrate, but are mentioned now to provide a benchmark for the current study.

Schroder's work was the first in the line of research and utilizes the photonic sintering system to determine resistivity of silver and copper nano ink sintered onto Mylar. Figure 6 is the resulting graph of resistivity of the silver film as a function of areal energy density. Typical energies required to cure films of silver nano ink onto Mylar were found to be 500 – 2000 mJ/cm<sup>2</sup>.

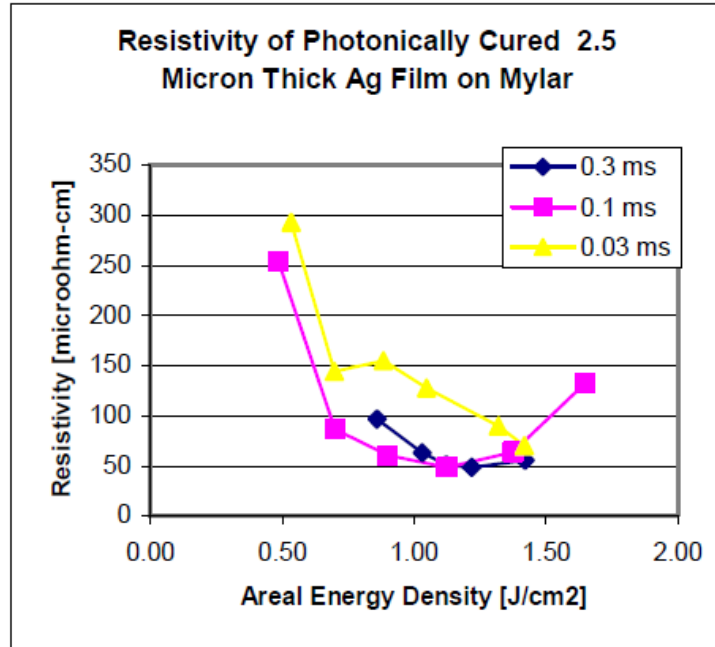


Figure 6. Resistivity of Photonicallly Cured 2.5  $\mu\text{m}$  Thick Nano Silver Ink Film on Mylar [12].

The ink was applied to the substrate using a wire wound rod. It is reported that the curing of silver films occurred on a variety of substrates including glass, however results for these substrates were not presented.

The work of West et al. (2012) evaluated the effectiveness of photonic sintering of silver nanoparticle depositions, and was done by measuring the densification of silver nanoparticles. The process of measuring densification was accomplished by comparing calculated densities before and after the sintering process. Ink was deposited in a 3 mm by 10 mm pad on a slide and then weighed to obtain the mass component of the density calculation. Then, using a Zeiss Imager M1M microscope, the thickness of the deposition was measured for the volume component of the density calculation. The results show that

the optimal densification of a 35  $\mu\text{m}$  thick silver nanoparticle deposition is achieved by a setting of 1200V for 900  $\mu\text{s}$  using a Novacentrix PCS-1100 Photonic Curing System. It was also observed that voltages greater than 1600 V produced cracking in the films and was taken as an upper limit for the voltage setting with the chosen pulse length [18].

Figure 7 illustrates the results.

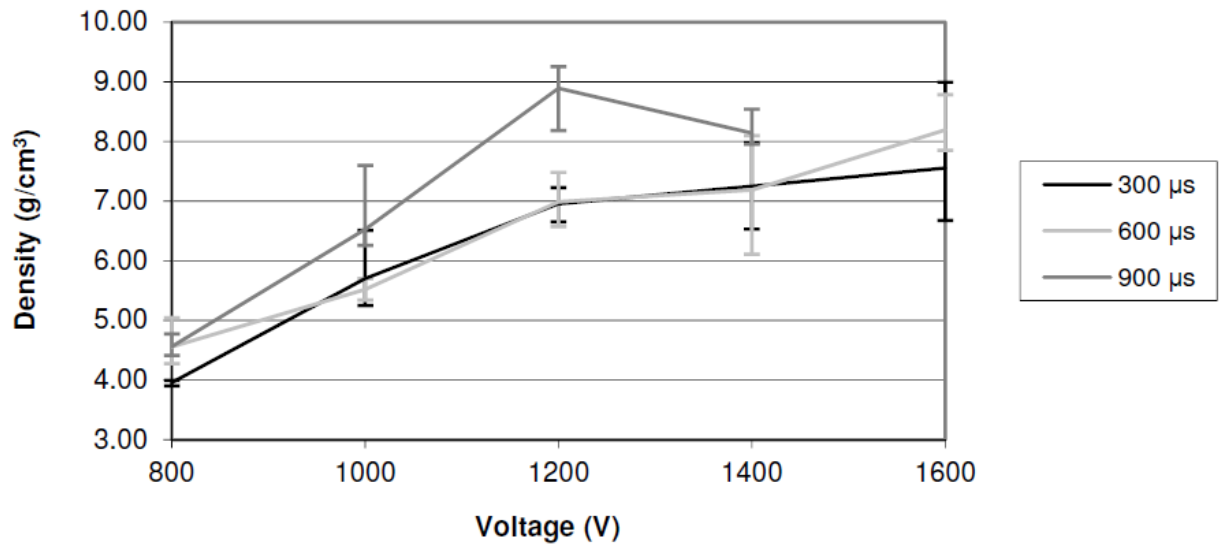


Figure 7. Densification of a 35  $\mu\text{m}$  Silver Nanoparticle Film on Glass. [18]

### Quality Testing

Generally, quality testing will mean different things depending on what is entailed in the printing process, the curing process, and are the critical characteristics of end product.

Critical characteristics of both electronics and printing are present, and two of the

important ones include adhesion of the cured film to the substrate, and sheet resistance of cured film.

## Adhesion

Adhesion is the first performance test for quantifying the effects of the change in sintering parameters and presence of frit

An important consideration to the adhesion of ink on substrate is the substrate itself and the treatment of the substrate before sintering. Treating the substrate can impart desired properties, such as hydrophobicity or hydrophilicity. Each characteristic will influence the degree of interaction at the ink/substrate interface, and both characteristics can be quantified by the contact angle.

The contact angle is the angle created by the intersection of the liquid-solid interface and the liquid-vapor interface (geometrically acquired by applying a tangent line from the contact point along the liquid-vapor interface in the droplet profile [22]). Figure 8 illustrates this angle as the lowercase Greek letter theta ( $\theta$ ). A surface treatment that effectively minimizes the contact angle without affecting the printability is desirable for adhesion [23]. To explain, an understanding of the thermodynamic work of adhesion is necessary. Work of adhesion may be defined as the reversible work per unit length to separate two phases that initially have a common interface [23].



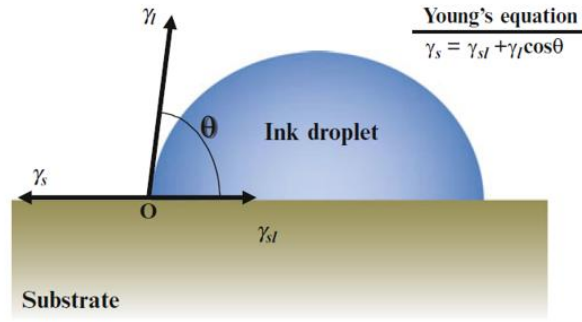


Figure 8. Contact Angle of Ink Droplet on Substrate [2].

Necessary for the theoretical calculations for the work of adhesion ( $W_A$ ) is the surface tension and contact angle. Using Young's equation presented in Figure 8 for the solid and liquid interface surface tensions, and the Dupré's energy equation (Equation 6) the adhesion of ink to substrate can be calculated [24].

$$W_A = \gamma_s + \gamma_L - \gamma_{sL}$$

Equation 6

Where  $W_A$  is the work of adhesion (mN/m)

$\gamma_s$  is the solid interface surface tension (mN/m)

$\gamma_L$  is the liquid interface surface tension (mN/m)

$\gamma_{sL}$  is the solid/liquid interfacial tension (nN/m)

The combination Young's and Dupré's equations lead to Equation 7.

$$W_A = \gamma_L (\cos\theta + 1)$$

Equation 7

Where  $W_A$  is the work of adhesion (mN/m)

$\gamma_L$  is the liquid interface surface tension (mN/m)

$\theta$  is the contact angle

The smaller the contact the greater the work of adhesion. The advantage of this equation is that calculation of  $W_A$  is based only on  $\gamma_L$  and  $\theta$ , which are experimentally relatively easy to determine. Contact angle was not determined because the aim of the study is quantification of adhesion post sintering.

Post sintering adhesion is a function of both contact angle of the ink and the densification process as described in chapter 0. In order to study adhesion post sintering, mechanical forces were applied to the film in a way that the film remaining is a measure of adhesion. Such is the focus of chapter 0.

## Resistivity

Resistivity will be the second performance test for quantifying the effects of the changes in sintering parameters and presence of frit. The most common way to measure a material's resistance is by a four point collinear probe. The sheet resistivity measurement, (the measurement on resistivity per square unit distance) is possible with an array of four equidistant probes. Figure 9 illustrates the array with the probes providing the current

source on the outside of the probes to measure the voltage drop. The sheet resistivity is a result from Equation 8.

$$\rho = \frac{\pi}{\ln 2} \times \frac{V}{I} \times b \times k$$

Equation 8

Where  $\rho$  is sheet resistivity (Ohm/cm)

$V$  is the measured voltage (volts)

$I$  is the source current (amps)

$b$  is the sample thickness (cm)

$k$  is a correction factor based on the ratio of the probe spacing to wafer diameter and the ratio of wafer thickness to probe spacing [25].

Differences in film thickness were assumed negligible, thus the correction factor was calculated to be 3.59  $\Omega/\text{sq}$  using standard four point collinear probe test procedure [25].

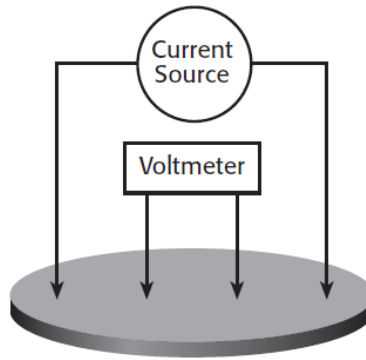


Figure 9. Keithley Four Point Probe for Measuring Resistivity. [25]

Resistivity of silver films of thickness greater than 45 nm annealed to ITO under vacuum with temperatures ranging from 50 – 500 °C has been shown to have values in the  $10^{-6}$  -  $10^{-5} \Omega/\text{cm}^2$  range [18].

## CHAPTER III

### EXPERIMENTAL METHODS

#### Design of Experiment

The design of experiment (DOE) is a combination of two  $2^2$  full factorial designs. Each was such that the adhesive characteristics and resistivity of the silver nano ink films

printed on ITO coated glass specimens with and without adhesion promoting glass frit (VS1307) can be analyzed for 2 different sets of sintering parameters. The first experiment investigates adhesion and resistivity of specimens with and without the (VS1307), and a relatively high amount of energy ( $\text{mJ}/\text{cm}^2$ ) and a relatively low amount of energy, and are represented by +1, -1, E+1 and E-1 in experiment 1 of Figure 10 respectively. The second experiment investigates adhesion and resistivity of specimens with and without VS1307, and a relatively fast sintering speed ( $\text{ft}/\text{min}$ ), and a relatively slow sintering speed, and are represented by +1, -1, S+1, S-1 in experiment 2 of Figure 10 respectively.

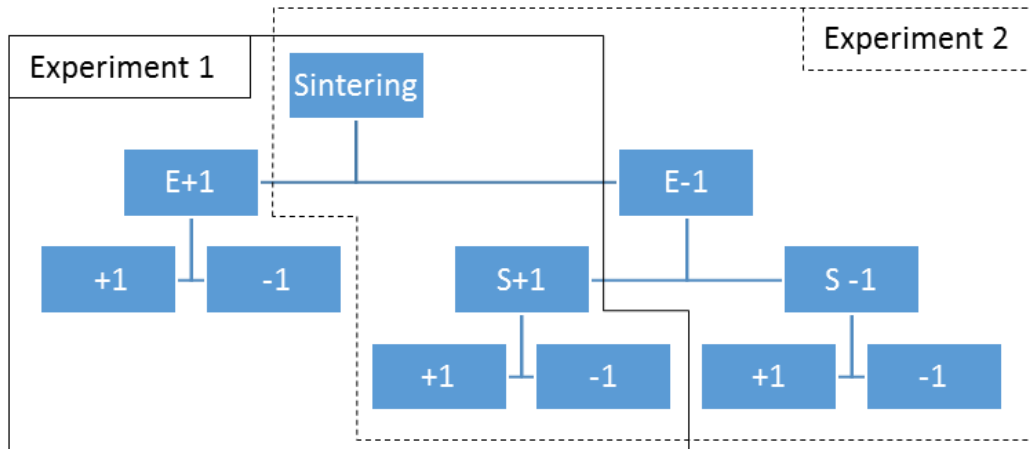


Figure 10. Design of Experiment

## Surface Preparation

The different baths were used, each containing a different cleaning agent. Bath 1 contained aqueous trichloroethylene, 98%, purchased from Alfa Aesar, a Johnson Matthey Company, Heysham, England. The lot number is 10181505. Bath number 2 contained Crown Brand acetone, a Sundry Chemical Company. Bath number 3 contained Crown Brand isopropyl alcohol.

The choice of substrate was ITO coated glass obtained from Gentex Inc., Zeeland, MI. The glass measured 100 by 110 by 1.5 mm, and only one side is coated with the ITO.

The ITO glass substrate was first cleaned using a sequence of 3 consecutive baths. Bath 1, Bath 2, and Bath 3 contained trichloroethylene (TCE), acetone, and isopropyl alcohol, respectively.

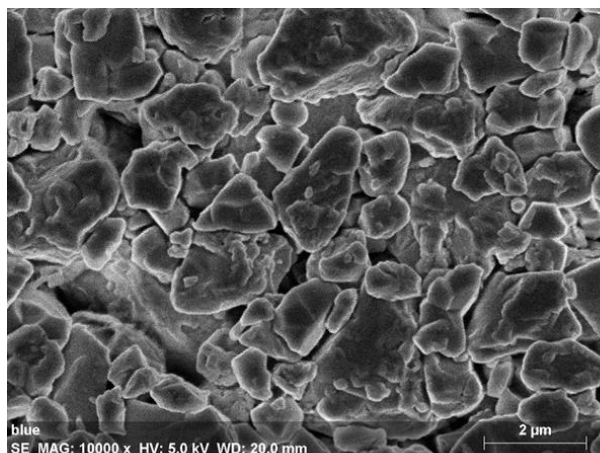
The bath dimensions were such that the substrate would sit flat, unobstructed by the edges of the container. This measure was taken to ensure that the entirety of the print-side surface, defined as the side of the substrate that the thin film would adhere to, could be covered by the same amount of cleaning agent. The specimen sitting flat would also allow for minimization of stresses, which could create the potential of breakage.

The amount of cleaning agent added to each bath was a standard volume of 500 mL, chosen to completely submerge the specimen. The bath containers used were sized to fit 5 plates side by side. The number of plates per bath was limited to 5. With a standard volume of cleaning agent above the surface of each plate sitting flat to the horizontal, and

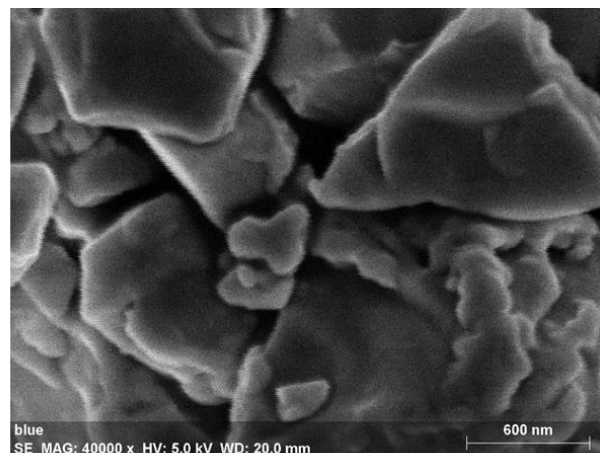
a limit to the number of plates per bath, saturation of the cleaning agent with foreign substances was assumed negligible. The plates were submerged for 5 minutes per bath.

### Printing

The adhesion promoter under study was the VS1307, and was supplied by Hitachi Chemical Co. America. VS1307 contains 40 – 60% glass frit (CAS No. 65997-17-3), 15 – 25% Ceramic (CAS No. 66402-68-4), 1-5% ethyl cellulose (CAS No. 904-57-3), 1-10% 2-phenoxyethanol (CAS No. 122-99-6) and 40 -60 % terpineol (CAS No. 8000-41-7) [26]. Figure 11 is an image of VS1307 captured from a scanning electron microscope. From the image, the all solids contained within the VS1307 are cuboidal.



A.



B.

Figure 11. Scanning Electron Microscope Images of VS1307 at Different Magnification, Courtesy of Western Michigan University Chemistry Department.

The viscosity of the VS1307 at the aforementioned compositions was too viscous to print with using the Harper QD Phantom proofing press, thus additional terpeneol was added to the VS1307 mixture in order to allow for adequate printing. The additional terpeneol was purchased from Aldrich, St. Louis MO, Lot # BCBL0327V. The mass composition of the mixture of VS1307 and additional terpeneol was 55% VS1307 and 45% terpeneol, making the composition of glass frit approximately 27.5 – 33 % glass frit.

The ink used throughout the experiment was PFI-722 Silver Flexographic Ink, purchased from Novacentrix, Austin, TX, PFI-722 is intended to be used for printed electronic applications. PFI-722 is a water based ink containing 60% by weight silver Nanoparticles (CAS No. 7440-2-4). The ink also contains 1-5% and 2% proprietary adhesive and proprietary rheology additive respectively. The remaining component is water.

When not printing, the PFI-722 was kept in cold storage for the purposes of preservation of the solvent. Cold storage minimizes losses due to evaporation. One additional advantage of the cold storage is the minimization of ink exposure to light.

The substrate was first determined to be the ITO coated side through the use of a common Digital Volt-Ohm Meter (DVOM). The DVOM was set to resistance and the leads were gently placed to on the same side of the plate. A measureable reading of conductivity indicated that the corresponding side of the plate was the ITO coated side. The ITO side would then be placed up on the press bed for printing.



The proofing press used for the study is a QD Phantom Flexographic Proofing press, developed by Harper Scientific, Charlotte, NC. The proofing press is designed to be used for laboratory scale use, the minimal utilities needed also make the press portable.

The press is comprised of three main components, the press bed, the carriage assembly, and the variable speed carriage rail mechanism. The press bed is the rest fixture for substrate on which the printed film is applied. The press bed provides force on the substrate in the opposite direction as the carriage assembly, allowing the ink to transfer from the carriage assembly to the substrate. The carriage assembly, Figure 12; is made up of the carriage, transfer roller, anilox roll, and the doctor blade. It is this assembly that works as the flexo printing system illustrated in Figure 12 [27].

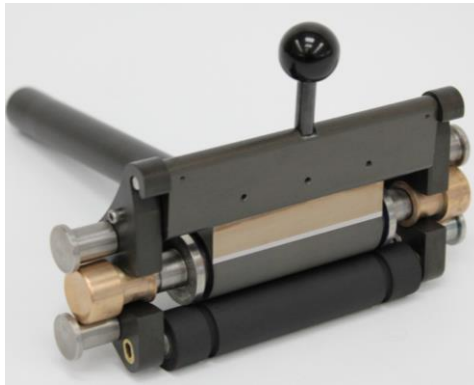


Figure 12. Harper Scientific Carriage Assembly with Rubber Transfer Roll [27]

The carriage assembly used was provided with interchangeable anilox rolls of varying billion cubic microns per inch (BCM), including 1200, 800, 500, and 440 BCM.

Constants for the DOE included the carriage assembly utilized a non-image transfer roll, the springs applying the pressure to the carriage assembly (spring constant = 9lb<sub>f</sub>/ft), and the speed (135 inches per minute).

The ink used removed from the cold storage 30 minutes prior to printing. Printing was done per Harper Scientific instruction. Printing of the thin film consisting of either the PFI-722 and/or modified VS1307 mixture was completed with flexographic proofing press.

Printing was completed layer by layer after a partial drying time. Each layer beneath the top layer was printed and allowed to partially dry for 1 day before printing each additional layer in a climate controlled room kept at 23 °C and 60% relative humidity. This partial drying allowed the bottom layer to remain intact whilst the additional layer was printed. Once all layers were present, the specimen was immediately subjected to the photonic curing process.

### Photonic Curing

The photonic curing equipment used was a Pulse Forge 1200 manufactured by Novacentrix, Austin, TX. It utilizes a water cooled xenon lamp, capable of producing energies of up to 21 J/cm<sup>2</sup>. The machine utilizes a software interface called Pulse Forge. Pulse Forge allows for the changing of key parameters that affect the sintering process. These sintering parameters are:

1. Voltage – The voltage supplied to the sintering lamp.

2. Envelope Duration – Total time for a set of micro pulses used to photonically sinter the chosen sample, and the rest time between pulses.
3.  $\mu$  Pulses – The number of pulses of light from the lamp
4. Duty Cycle – The ratio of time the flash lamp is on to the time the flash lamp is off.
5. The PulseForge 1200 is a water cooled unit fully capable of adjustments of the key machine settings.

The temperature distribution in the film stack is controlled by adjustment of key machine settings. Machine settings include lamp voltage (volts), envelope duration, number of micro pulses, duty cycle. In addition to these machine settings, the motion of the specimen during the lamp operation can be changed to accommodate (once through) web speeds of up to 20ft/min. During operation, the specimen and stage move directly under the sintering lamp. The lamp then discharges a particular predetermined amount of stored electromagnetic energy, which is absorbed by the specimen. The discharge rate can be varied by changing a machine parameter entitled “fixed position.”

The sintering parameters were under investigation for the proof of concept. Table 3 is a summary of the sintering profiles and the associated parameters. Not included in Table 3 is the distance between stage and flash lamp, which was held at 20 mm for all specimens.

Table 3. Sintering Profiles for Novacentrix PulseForge 1200 Used for Proof of Concept.

DOE Factors	Voltage	Pulse Length	No. of $\mu$ -pulses	Envelope	Duty Cycle	Mode	Stage Speed	Overlap Factor	Energy
Energy	Volts	ms	n/a	n/a	n/a	n/a	ft/min	n/a	mJ/cm <sup>2</sup>
Speed									
E+1	440	9000	1	10000	0.90	once through	5	2.0	14130
S-1									
E-1	330	450	1	500	0.90	once through	5	2.0	900
S-1									
E-1	330	450	1	500	0.9	once through	20	1.0	900
S+1									

### Adhesion Testing

The adhesion as discussed earlier can be modeled by theoretical means, but given the complexities of the adhesion process, it is reasonable to state that presently no test can precisely assess the actual physical strength of an adhesive bond. There is, however, a way to obtain an indication of relative adhesion performance [28], [29]. For this reason, currently practiced industry standards were considered to provide a method of measuring adhesion. The method utilized by both the automotive glass and printed electronic industry, alike, is the cross cut method as outlined by ASTM D3359 [14], [30], [31]. The standard describes two methods suited for either field work or laboratory work. The laboratory method was chosen in this study for assessing the adhesion of the silver nano ink to the glass substrate after sintering.

The assessment of adhesion is made by a three step process:

1. Scoring a series of 22 lines centered in a grid pattern (11 lines x 11 lines) by means of a razor;
2. Applying a special adhesive tape to said grid, and rapidly removing it at a 180° pull angle. The tapespecified by the standard, Permacel P99, has been discontinued, therefore the replacement tape, called CHT tape, developed by SEMicro, Rockville, MD, was used. The two tapes are very similar in specifications. Table 4 highlights the similarities of force exerted per inch when the tape is placed on the sample for 90 s, as well as shelf life. CHT provides similar results according to the results of independent testing performed by ChemsSultants International of Mentor, OH [32].

Table 4. Comparison of Tapes Used for ASTM D3359 [33].

<b>Material</b>	<b>Adhesive Type</b>	<b>90 sec Peel Test [oz/in]</b>	<b>Shelf Life [months]</b>
Permacel P-99	Synthetic Rubber	61	12
SEMicro	Synthetic Rubber	59	12

3. The percentage of ink that is removed by the tape is then quantified. The adhesion is categorized in 1 of 5 different ways, and is based on the percentage of ink film that is removed from the substrate. The area removed ranged from less than 5% to greater than 65%, and the respective classification criterion is 5B to 0B [34]. Figure 13 is the classification table of 5B – 0B with examples of each under the heading Surface of Cross-Cut Area From Which Flaking has Occurred for Six Parallel Cuts and Adhesion Range by Percent. 0B exhibits the most flaking, whereas 5B has the least representing poor and excellent adhesion of the film respectively. ASTM D-3355 proved ineffective at comparing the adhesion strength of either parameters of the DOE. The problem was that it did not remove any of the film. The cross cut method was abandoned for another means of relative adhesion.

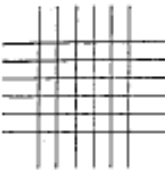
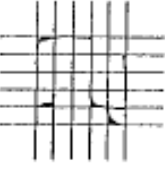
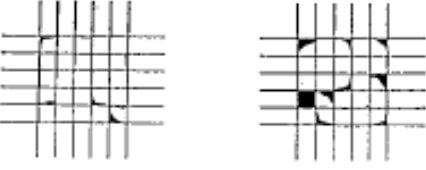

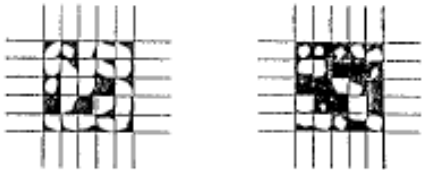
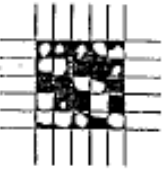
CLASSIFICATION OF ADHESION TEST RESULTS		
CLASSIFICATION	PERCENT AREA REMOVED	SURFACE OF CROSS-CUT AREA FROM WHICH FLAKING HAS OCCURRED FOR SIX PARALLEL CUTS AND ADHESION RANGE BY PERCENT
5B	0% None	
4B	Less than 5%	
3B	5 - 15%	
2B	15 - 35%	
1B	35 - 65%	
0B	Greater than 65%	

Figure 13. Classification of Adhesion Results [34].

Due to the inability of the cross cut test to provide a measure of relative adhesion, a new method was needed. Quantifying adhesive characteristics shifted from the force needed to remove the film from the substrate, to the film's resistance to abrasion. Such a test is

similar to TAPPI T-467 standard, utilizing a Taber 5130 Abraser, manufactured by Taber, North Tonawanda, NY.

The Taber 5130 is a device that spins a specimen resting on a turntable on a central vertical axis, while applying an abrasive force via 2 abrasive discs (CS-10 Calibrase Wheels) that also rotate at on a perpendicular axis. The axis of rotation of the abrasive wheels is displaced from that of the turntable creating an abrasive “sliding” action as the specimen rotates.

Figure 14 is an illustration of the abrasive action utilized by the Taber 5130. The abrasive wheel provide the wear area of  $300 \text{ mm}^2$ . The arms alone applied 0.25 N to the abrasive wheel, and no additional weights were added [35]. The turntable rotated at 72 revolutions per minute.

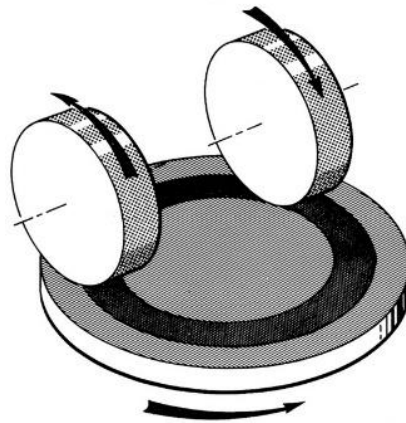


Figure 14. Abrasion Action Utilized by Taber 5130 [35].



Preparation of the Taber specimen began with cutting the sample to an average size of 105 x 100 mm. Then a center hole through the specimen was bored to accommodate the center spindle of the Taber 5130 which can be seen in

Figure 15. This center spindle hole was drilled using a Dremel brand Model 395 type 5 rotary grinder equipped with a carbide conical bit. The grinder was set for 30,000 rpm, and steady pressure was applied manually to the specimen to create the center spindle hole.

The TAPPI T-476 standard outlines a test for the resistance of surface to the act of abrasion. The way to achieve this is by a mass method. The mass of the specimen is measured before and after being subjected the abrasive wheels, and is then compared to provide a relative measure of the film's adhesion [36]. This was not chosen due to variation in the registration of subsequent layers (

Figure 15). Small variation in the position of each layer in reference to one another creates variation in area subjected to abrasive wheels, thus an alternate method was needed.

An alternate method to characterize resistance to abrasion can be achieved by clearly defining an end point for abrasion. This occurs as the specimen being subjected to the abrasive wheels until a particular condition is observed. This also was not chosen, rather, the number of revolutions each specimen was subjected to the abrasive wheels for was fixed and chosen based only a partial exposure of the substrate. The number of revolutions was fixed at five, which provided enough abrasion such that both the

remaining printed film and the ITO coated glass substrate was visible to the naked eye. The partial exposure of the substrate would then be analyzed.

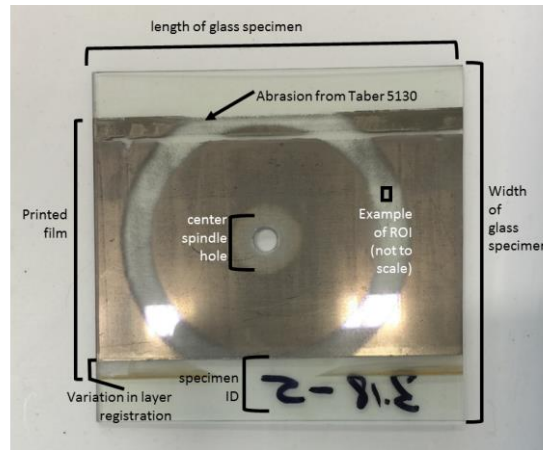


Figure 15. Sample Diagram of Taber Test Specimen

The method used to analyze the partial exposure of glass of each specimen was achieved with software and a camera-based solution developed by ImageXpert, Nashua, NH. The software is an automated visual system that evaluates changes from light pixels to dark along a grey scale ranging from 0 (black) to 255 (white). The software utilizes an algorithm to calculate the percentage of area still covered by the printed film. The threshold, or grey value that divides light pixels from dark pixels, was determined by placing a specimen at the edge of glass substrate and printed film, then adjusting the grey value until there is a clear distinction between glass and printed film. Figure 16 illustrates the appropriate threshold, with the top half representing the bare glass, and the lower half

representing the untouched printed film. The inclusion of the histogram in Figure 16 shows at what gray tone represents the bare glass. Figure 17 is an example of the type of comparison of specimens post abrasion as analyzed by the Image Expert software for the Percent glass exposed. Figure 17.A illustrates a specimen with low percent film, relative to that of the specimen in Figure 17 B. The greater the percent film that has been removed from the abrasion test, the greater the number of light pixels (top half of Figure 16).

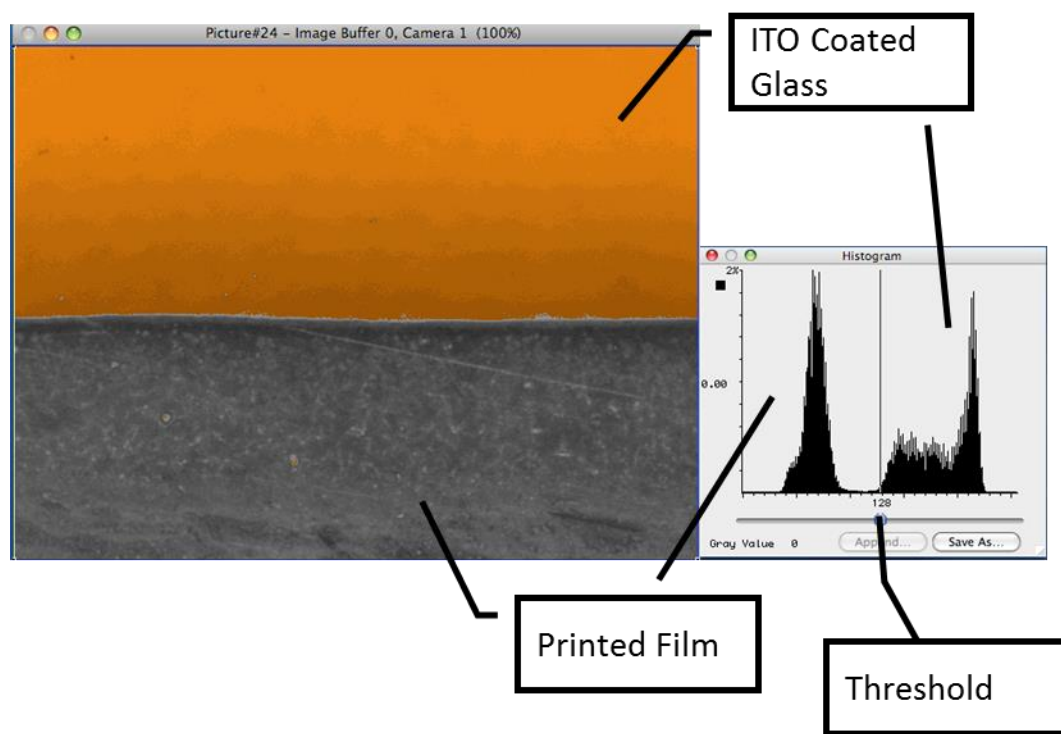


Figure 16. ImageXperts Analysis: Determining Glass from Printed Film.

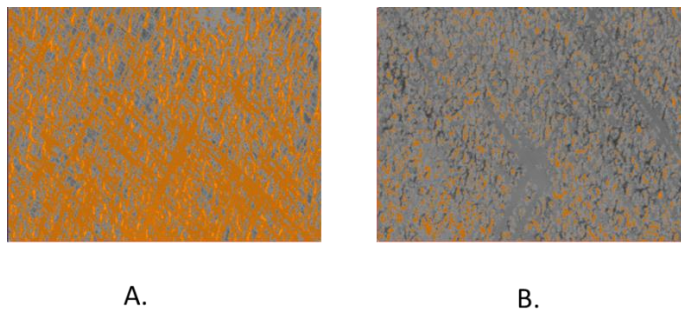


Figure 17. Comparison of Specimens Post Abrasion Analyzed by Image Expert Software for Percent Glass Exposed

For each specimen, nine random regions of interest (ROI) were chosen for analysis. The ROI was 640-480 pixels and positioned within the abraded area by the Taber 5130.

### Resistivity

Resistivity of the printed film/substrate was determined through the use of a Keithley 2400 Source Meter. The mean of 9 readings, taken in a grid pattern as seen in Figure 18, makes up the resistivity measurement of each specimen. The grid spacing is approximately 2 cm in both directions. The total film dimensions were on approximately 7 x 11 cm.

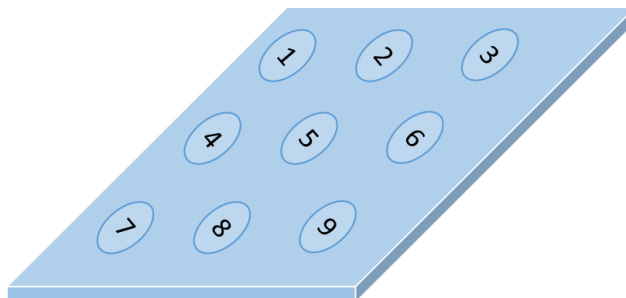


Figure 18. Schematic for Average Resistivity Measurement

## CHAPTER IV

### RESULTS

Prior to adhesion and resistivity testing, scanning electron microscopy was performed to qualify the differences in adhesion and resistivity. Figure 19.A is the printed silver nano ink film printed on ITO coated glass, and Figure 19.B is the same printed silver nano ink film on ITO, but with the addition of a VS1307 layer. VS1307 is evident in the sample by the presence of larger glass frit particles. Comparison of the processed VS1307 (i.e., printed and sintered) with that of VS1307 in its raw form, as presented in Figure 11, clearly shows that enough energy was applied during the sintering process to melt the glass frit particles. This is evident by the size reduction and deformation of the particles.

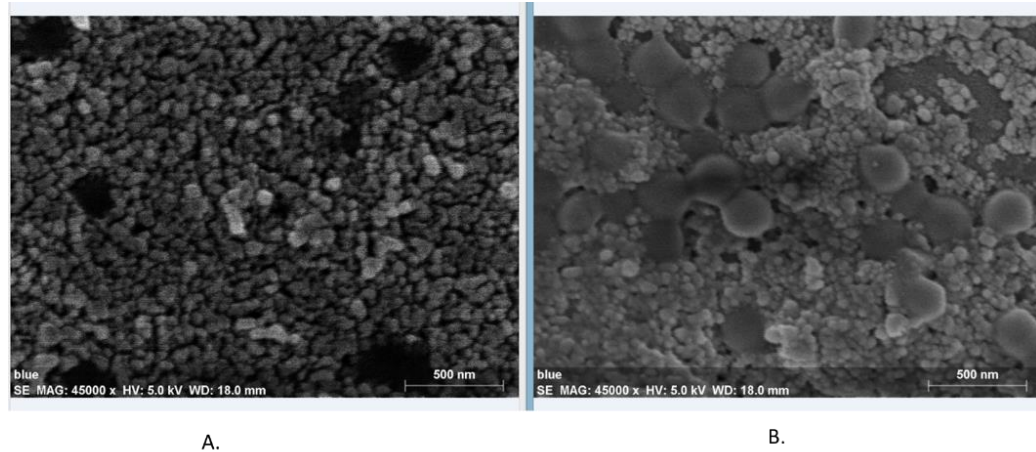


Figure 19. Scanning Electron Microscope image of (a) without VS1307 and (b) with VS1307.

Comparison of the two images in Figure 19 clearly shows there is a decrease in the number of voids in the presence of VS1307. This densification of the sintered film is in agreement with the results obtained by Jang, et al. (2008). The key difference between the two is the method by which they were sintered, Jang used a conventional thermal chamber heated to sintering temperatures, while the research presented here was sintered by means of flash lamp or photonic technology.

For any experiment, model adequacy must always first be considered. It is assumed that the error embedded in the experiment is normally distributed, which becomes important when performing analysis of variance for the data. Departures from normality usually causes the significance level of the factors, i.e., sintering parameters and presence of VS1307 to differ from advertised values. Significance for effects studied in this experiment was based on an F-test.

A check of the normality assumption was made by constructing a normal probability plot using Minitab® Statistical Software. The plot is constructed by plotting the residuals against the normal percent probability. The residuals, the amount of variability in a dependent variable that remains after accounting for the variability attributed to any predictors in the analysis, resulted from the percent film remaining after subjugation to the Taber abrasion test and resistance measured by four point collinear probe. Figure 20 shows that error distribution is approximately normal as evident by the concentration of the residual data near the 50% mark and that they are approximately linear [37].

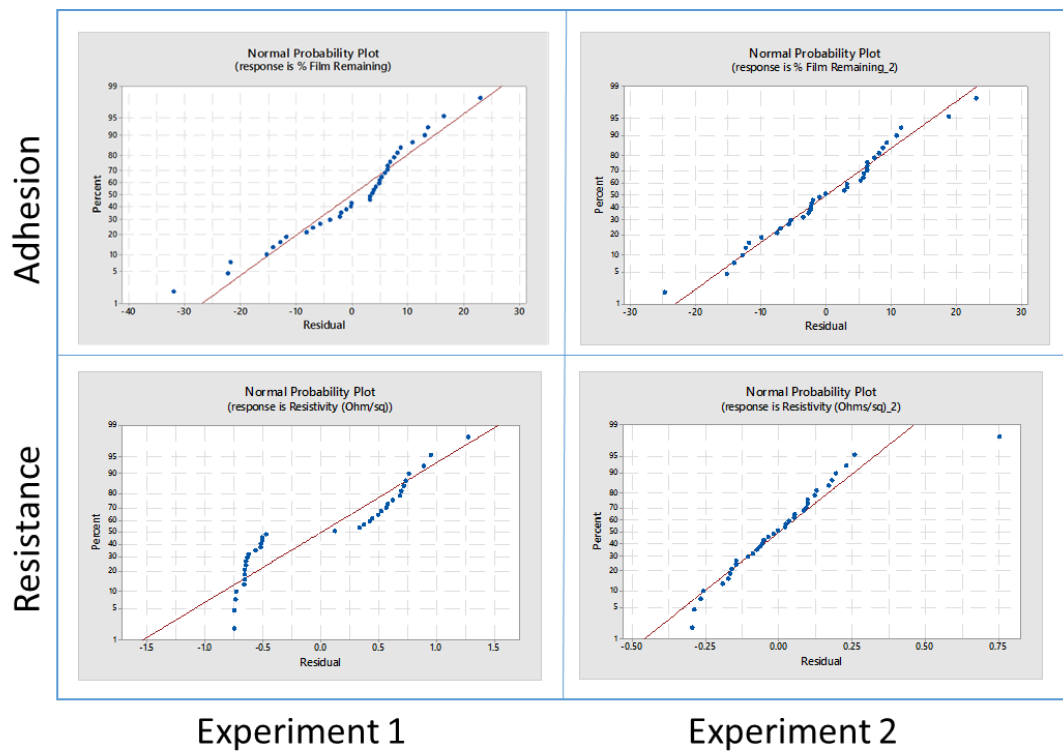


Figure 20. Normal Probability Plots for Percent Film Remaining and Resistivity for Experiment 1 and 2.

## Adhesion

The scope of this study is limited to the aforementioned DOE, however, additional samples were fabricated while altering one other independent variable, namely the anilox rollers used during the print process. Inclusion of this comparison only serves as a qualitatively consideration of the adhesion promoting properties of the VS1307.

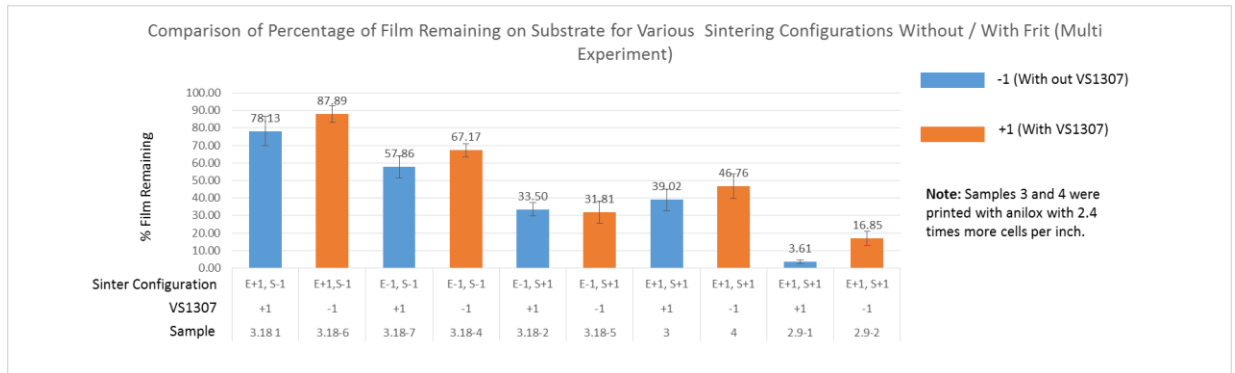


Figure 21. Multiple Experiment Comparison of Percent Film Remaining

Taber abrasion test proved adhesion promotion in all but two sets of specimens for a given sintering profile, that of the E-1, S+1 parameters. This sintering profile has a different stage speed, a speed in which the sintering stage and specimen move through the sintering process 5 times faster than that of S+1 and S-1, and can be seen in Table 3. Samples 3, 4, 2.9-1, and 2.9-2 were printed using anilox with 2.4 times more cells per inch than that of the ones used for the DOE. Additional research should be conducted to quantitatively compare the effects of VS1307 with the anilox variable.



Two trends emerge after analyzing the results of Experiment 1 and illustrated in Figure 22. Trend 1 is the average percentage of film remaining on the substrate after the Taber abrasion test is approximately 9.5% greater when the layer of frit was included. Trend 2 is that the increase from 900 mJ/cm<sup>2</sup> to 14130 mJ/cm<sup>2</sup> of energy applied during the photonic sintering process increases the percent of film remaining by approximately 20%.

For analysis of the DOE the hypothesis is percent film remaining is dependent on energy or presence of frit. The null hypothesis is percent film remaining is not dependent on energy or presence of frit. All means present throughout the study are data means and not fitted means.

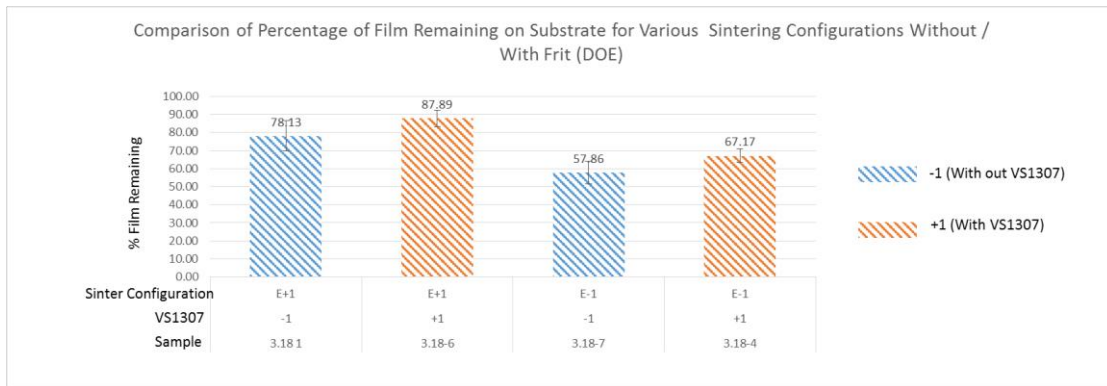


Figure 22. Comparison of Percentage of Film Remaining on Substrate for Changes in Energy, With/Without Frit.

Figure 23 is a main effects plot also describing trends 1 and 2. This plot compares side by side the effect of each factor has on the percent film remaining on the substrate. From this plot, one can easily see that of the given choices, the desired settings of +1 and E+1

should be chosen to provide a greater percentage of film remaining, or greater adhesive strength of the film.

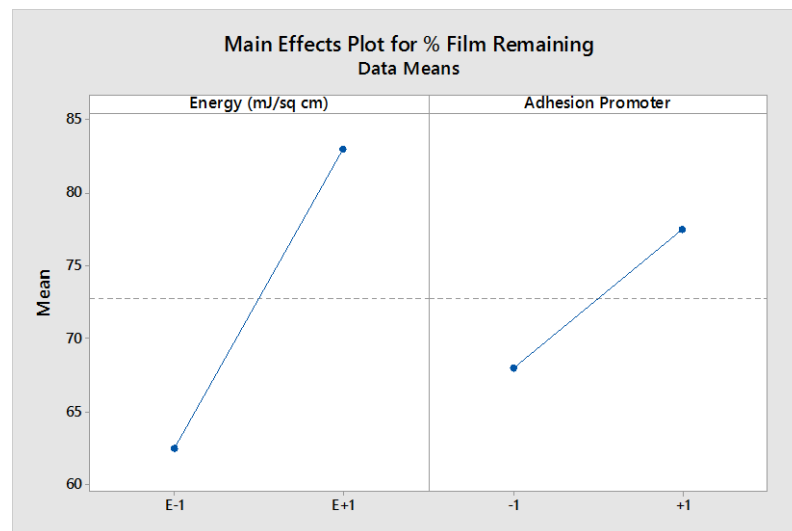


Figure 23. Main Effect Plot for Percent Film Remaining on Substrate for Experiment 1.

A determination of standardized effects was made for energy, the presence of the adhesion promoter (frit) and a possible interaction between the two using a significance level ( $\alpha$ ) of 0.05. Figure 24.A-B illustrate this using a Pareto chart and normal plot of standardized effect respectively. The model used for all main effects plots was the General Full Factorial Designs model and the associated analysis of variance tables are found in the Appendix.

The statistical significance of the factors was based upon evaluation of the p-value, or probability of obtaining a test statistic at least as extreme as the one actually calculated from the sample, if the null hypothesis is true. The p-value for the hypothesis is such that

it is too unlikely to have occurred by chance [38]. The interaction between energy and frit is however not statistically significant. Figure 24.A illustrates the energy is most statistically significant, as it has the greatest magnitude on the standardized effects scale.

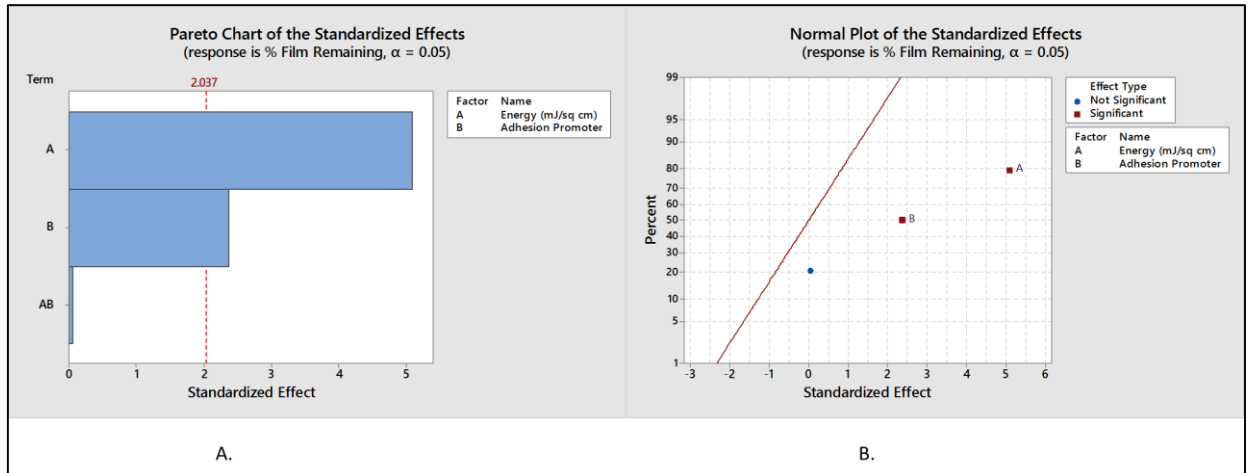


Figure 24.A) Pareto Chart and B) Normal Plot of the Standard Effects for Percent Film Remaining for Experiment 1.

Experiment 2 varied sintering speed and the presence of frit. Experiment 2 proved an approximate 30% increase in percent film remaining on substrate occurred for a decrease in sintering speed (Figure 25).

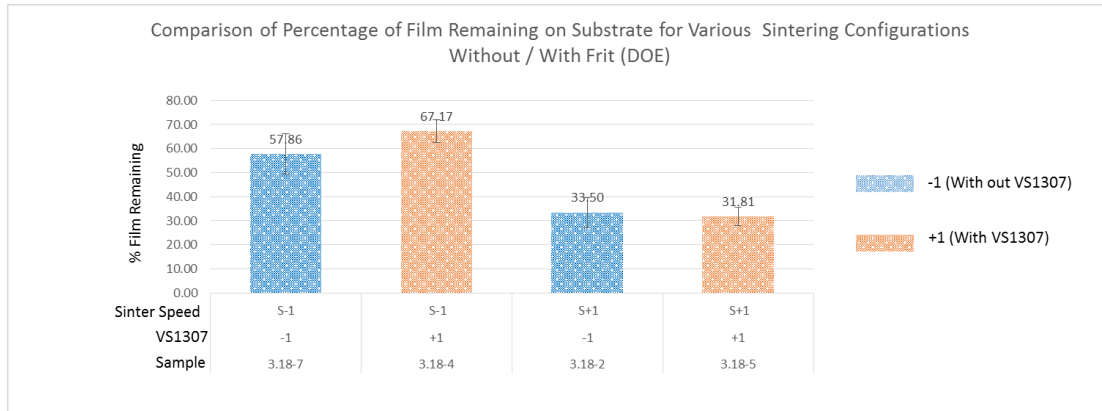


Figure 25. Comparison of Percent of Film Remaining at Different Print Speeds Without/With Frit.

As with Experiment 1, the main effects of Experiment 2 were analyzed as they relate to percent film remaining. As dictated by Experiment 2 of the DOE, the effects of stage speed and presence of the adhesion promoting glass frit are compared. From Figure 26, the percent of film remaining would be greatest if the sintering was done with a slower stage speed. It would seem that according to Figure 26 there is a slight increase in the percent film remaining should a layer of frit be present. However, analysis of standardized effects, (Figure 27.A-B), suggests that for Experiment 2, presence of frit or the frit's interaction with sintering speed does not have statistical significance as a standardized effect.

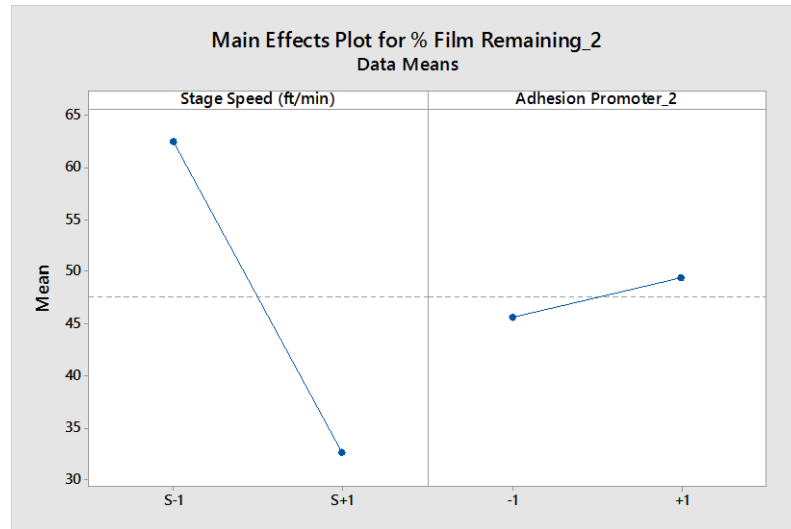


Figure 26. Main Effect Plot for Percent Film Remaining on Substrate for Experiment 2.

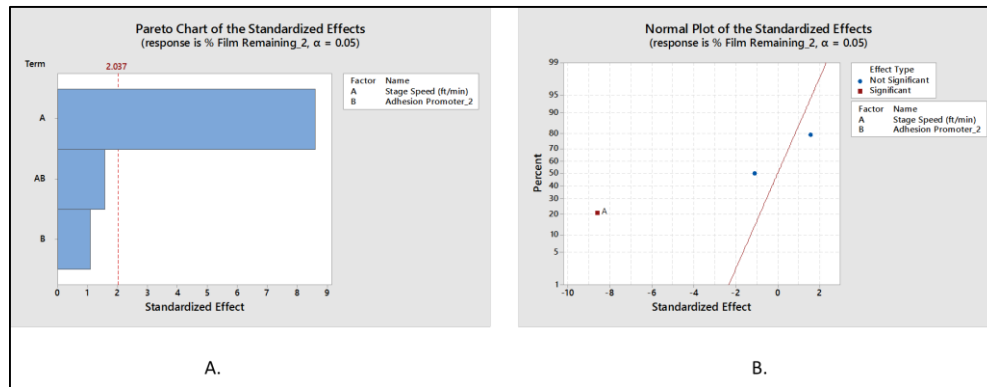


Figure 27.A) Pareto Chart and B) Normal Plot of the Standard Effects for Percent Film Remaining for Experiment 2

This contradicts the results of Experiment 1, in which the adhesion promoter was a standardized effect that is statistically significant. One theory for why the effect of the frit would differ between experiments is that with the increased sintering speed, insufficient

energy is absorbed by the frit to sinter to adjacent frit and/or silver nano particles.

Additional testing to confirm this theory is recommended.

### Resistivity

Resistivity for experiment 1 and 2 was analyzed in similar fashion to experiment 1 and 2 for adhesion. Hypotheses are defined as; the hypothesis is film resistance is dependent on sintering speed or presence of frit. The null hypothesis is film resistance is not dependent on sintering speed or presence of frit.

Considering Experiment 1, an increase in film resistance was exhibited for a decrease energy applied during the sintering process. Specimens sintered with an energy of 900 mJ/cm<sup>2</sup> presented on average 37 times higher resistivity than specimens sintered with 14130 mJ/cm<sup>2</sup>. This is a dramatic increase and is consistent with sintering theory. The greater the energy applied by the xenon light source, the greater the amount of energy absorbed by the silver nano particles, which results in greater surface area for contact after melting, and consequently, lower the resistivity. Figure 28 is a graphical representation of Experiment 1 as it relates to resistance, and includes the aforementioned energy/resistance relationship.

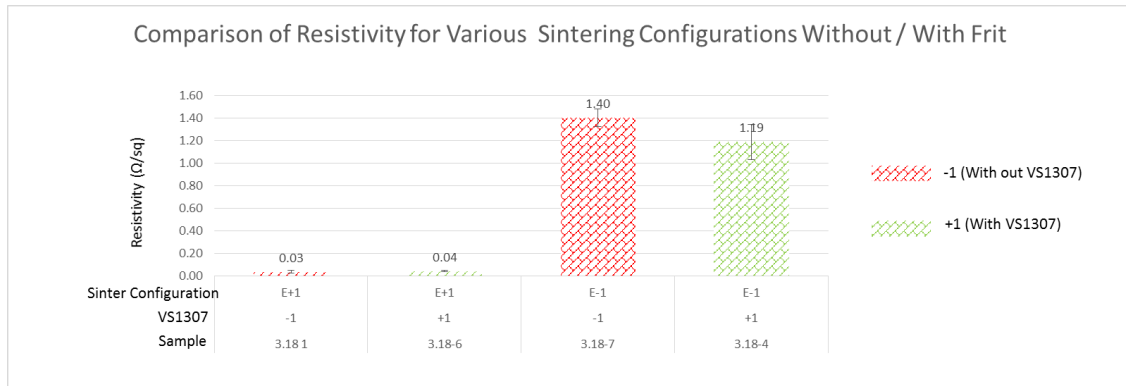


Figure 28. Comparison of Sheet Resistance for Different Energy, With and Without Frit.

It is important to note that resistance of the bare ITO coated glass was measured and was on average 2.75  $\Omega/\text{sq.}$ , which shows conductive functionality of all printed film, regardless of the presence of frit.

When looking at the associated main effects plot for resistivity as a function of energy and glass frit, Figure 29 the advantageous parameter for ensuring the lowest possible resistance is higher energy. Figure 29 also shows that addition of the frit layer can work to reduce film sheet resistance, but further analysis goes to show that presence of the frit layer is not statistically significant. Figure 30 shows this with A) a Pareto chart and B) normal plot of the standard effects.

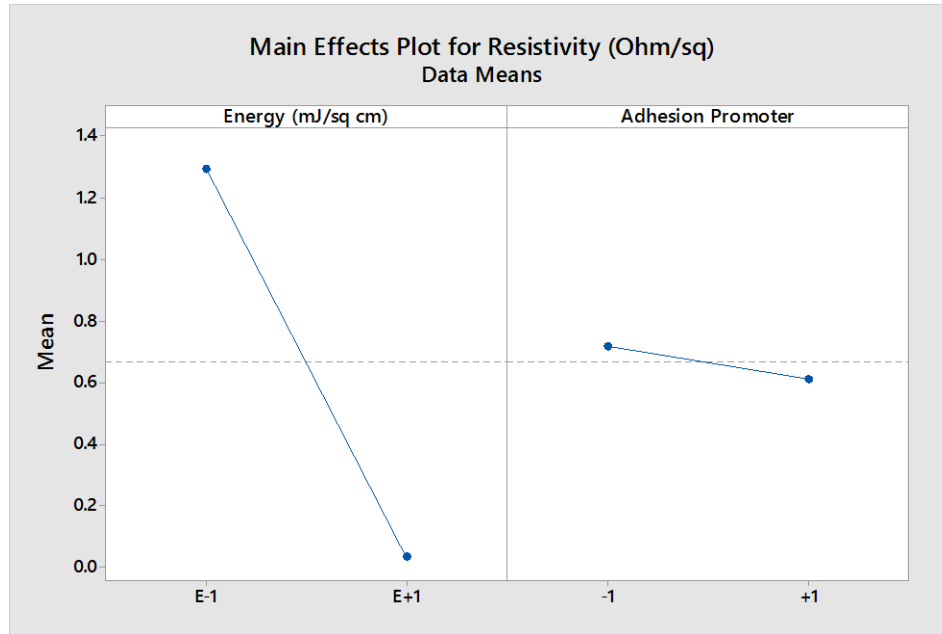


Figure 29. Main Effect Plot of Film Resistance for Experiment 1.

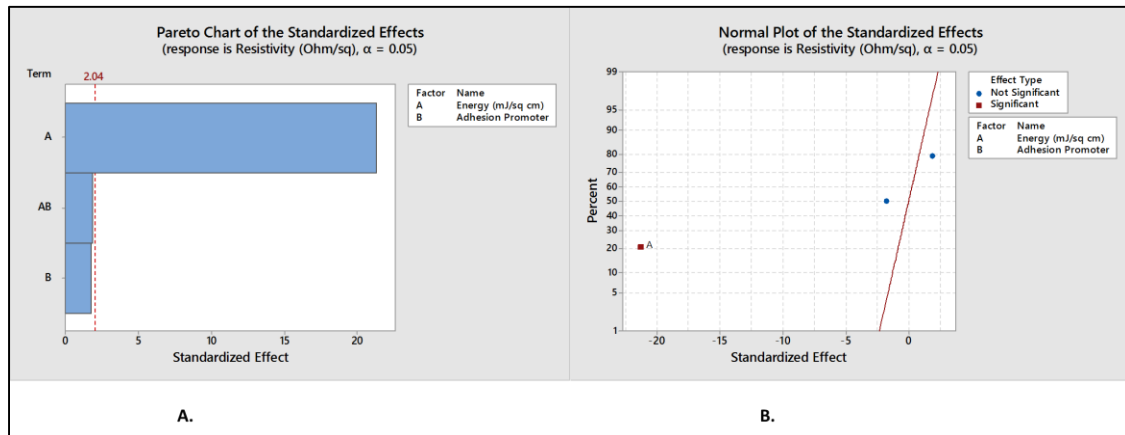


Figure 30.A) Pareto Chart and B) Normal Plot of the Standard Effects on Film Resistance for Experiment 1.

Analyzing film resistance as a function of sintering speed, with and without frit, (Figure 31), no clear trend(s) emerge. Across both sintering speeds (5 and 20 ft/min) and whether



the frit layer is present, film resistivity remains relatively close to a median of 1.24 ohms/sq, with a standard deviation of 0.46 ohms/sq.

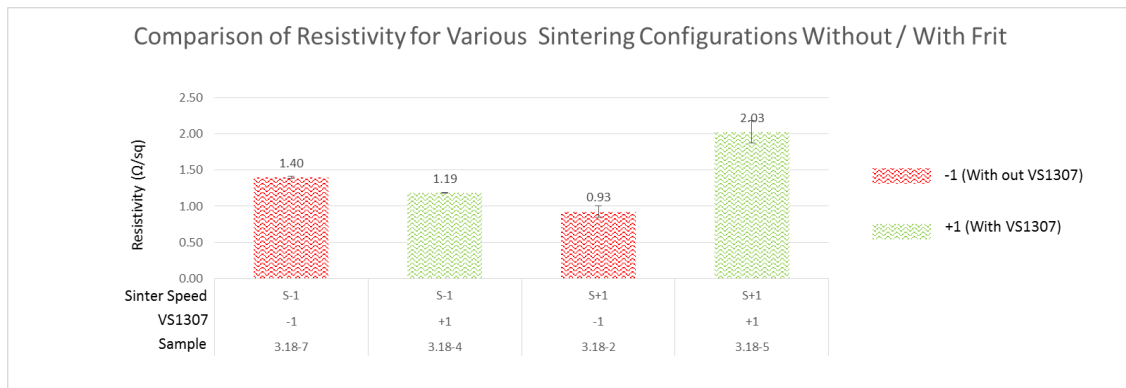


Figure 31. Comparison of Film Sheet Resistance for Different Sintering Speeds, With and Without Frit.

This would seem contrary to the main effects, Pareto, and normal standardized effects plots, (Figure 32, Figure 33.A, and Figure 33.B respectively). These plots show that there is a desirable set of parameters, and that both sintering speed and the frit presence is statistically significant. However, what Figure 33.A-B also illustrates the interaction between sintering speed and frit is also statistically significant and is the dominating effect.

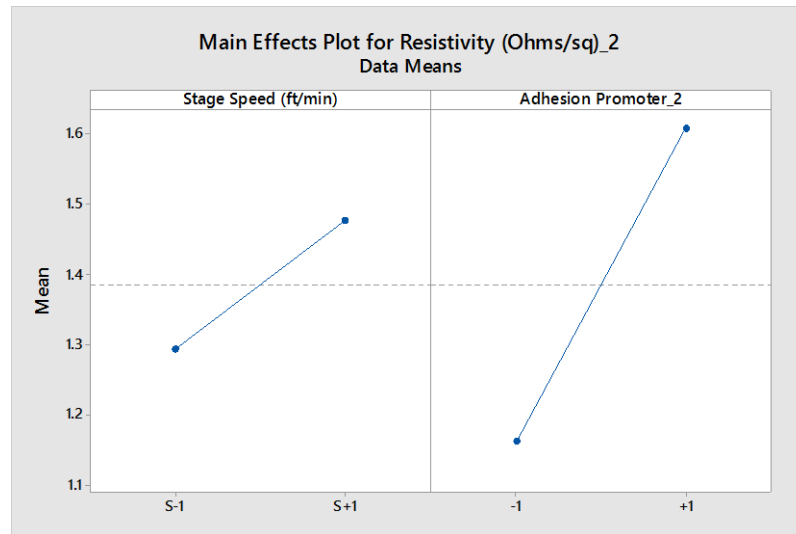


Figure 32. Main Effect Plot of Film Resistance for Experiment 2.

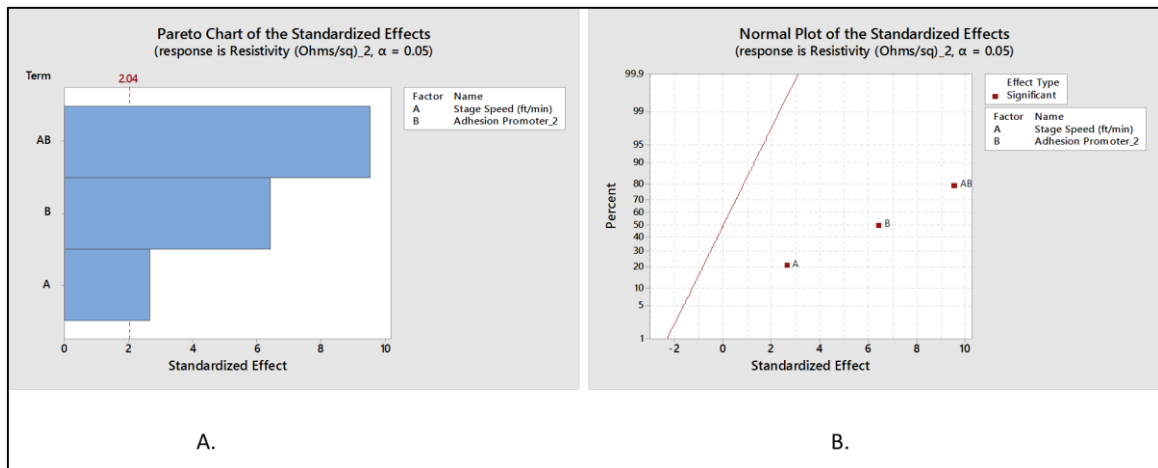


Figure 33.A) Pareto Chart and B) Normal Plot of the Standard Effects on Film Resistance for Experiment 2.

To analyze further, an interaction plot was generated, (Figure 34), in order to break into smaller components the effects of each variable. An interaction plot is a plot of means for each level of a factor with the level of a second factor held constant. The greater the

deviation from parallel lines, the greater the degree of interaction, and the intersecting lines in Figure 34 represents a strong interaction between the two factors [39]. The top right quadrant of Figure 34 shows that for S+1, resistivity decreases if a frit layer is present. It also shows that for S-1, resistivity increases less dramatically if a frit layer is present. The bottom left quadrant (BLQ) shows that for -1, resistance decreases with increasing sintering speed. The BLQ also shows that for +1, an increase in resistance for an increase in sintering speed. Considering both quadrants, a coveted low resistance could be facilitated by a fast sintering speed, (S+1) with frit (+1). This setup for optimum resistance has the opposite sintering speed as that of the optimum adhesion setup, frit is desired in both resistance and adhesion optimization.

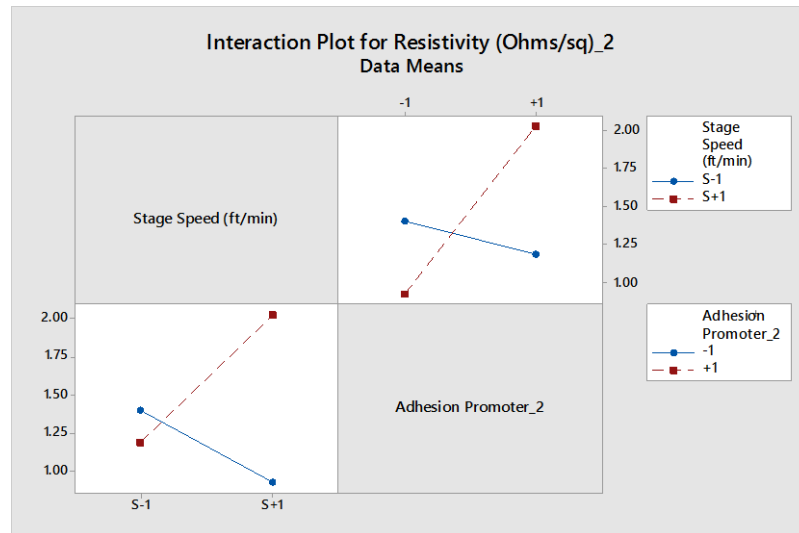


Figure 34. Interaction Plot of Sintering Speed and Adhesion Promoting Frit for Film Resistivity.

## CHAPTER V

### CONCLUSIONS

A process to produce printed conductive film on ITO coated glass using a photonic sintering/curing method was demonstrated. A conductive film was printed using silver nano particle ink and flexography onto an ITO coated substrate, then sintered using Novacentrix PulseForge 1200. An adhesion promoting layer containing 27 – 33 % low melting glass frit was printed using the same flexographic printing method to study its effect on adhesion. The adhesion was studied using a novel method that utilizes the combination of mechanical abrasion process and pixel analysis software. Resistance was studied with the aid of a four point collinear probe.

Adhesion improved with an increase in energy, and presence of frit, for which both factors were statistically significant. Adhesion decreases with increase in sintering speed.

Resistivity decreases dramatically for an increase in energy applied and presences of the adhesion promoter has no significant effect. A clear trend for resistivity as a function of sintering speed could not be observed.

## CHAPTER VI

### RECOMMENDATIONS FOR FURTHER STUDY

The study done concluded that energy was a significant factor in the adhesion and resistance of the printed conductive film. To expand this knowledge, a look into which of the sintering parameters has the biggest effect, and how each can be related to utility costs. For example, does the voltage or number of micro pulses have a significant effect? How does each affect the utilities cost? Also found to be a significant factor is the glass frit, a deeper investigation into the optimization of VS1307 composition that provides an increase in adhesion and decrease in resistance is a natural progression from this study.

Adhesion and resistance as a function of film thickness should also be studied. Film thickness can easily be varied by type of printing method used. If keeping with the flexo printing method, increasing the anilox BCM will provide insight on optimum film thickness.

Printing should also be performed in a clean room environment to prevent against the inclusion of particulate matter in the film. Particulates, such as dust, can cause discontinuities in the film, having adverse effects on both adhesion and resistance.

A printing registration system would benefit the adhesion testing. If all layers were registered with some high degree of accuracy, the analysis of the Taber 5130 abrasion test can be based on mass loss. This method is described in chapter 0.

The specimen hold-down mechanism on the Taber 5130 should be modified so that a through-hole does not have to be drilled through the specimen. Glass substrates are fragile and break very easily if not careful when drilling through them. The debris from the drilling process is also detrimental to the film being tested. To remedy this concern, a turntable with double sided tape to hold the specimen while keeping the entirety of the film intact should be implemented.

Lastly, to provide a high degree of accuracy for resistance measurements, future resistivity testing should be conducted using square specimens of a known thickness with tolerances providing a high degree of precision. Sizing the specimens to a fitted value for standard correction factors utilized by the four point collinear probe will also increase accuracy of the resistance of the film.

## REFERENCES

- [1] J. Perelaer, P. J. Smith, D. Mager, D. Soltman, S. K. Volkman, V. Subramanian, J. G. Korvink and U. S. Schubert, "Printed electronics: the challenges involved in printing devices, interconnects and contacts based on inorganic materials," *Journal of Materials Chemistry*, vol. 1, no. 20, pp. 8446-8453, 2010.
- [2] K. Suganuma, *Introduction to Printed Electronics*, New York: Springer, 2014.
- [3] E. Broitman, "What is the Best Way to Promote Adhesion Between Glass and Chromium?," 2013. [Online]. Available: [http://www.researchgate.net/post/What\\_is\\_the\\_best\\_way\\_to\\_promote\\_adhesion\\_between\\_glass\\_and\\_chromium](http://www.researchgate.net/post/What_is_the_best_way_to_promote_adhesion_between_glass_and_chromium). [Accessed 30th April 2014].
- [4] B. Kanegsberg and E. Kanegsberg, *Handbook for Critical Cleaning*, Portland, Oregon: CRC Press, 2001.
- [5] Serway and Jewett, *Physics for Scientists and Engineers Volume 2*, Mason, OH: Thomson, 2008.
- [6] R. A. Matula, "Electrical Resistivity of Copper, Gold, Palladium and Silver," in *J. Phys. Chem. Ref. Data*, 1979, p. 1161; 1209; 1260.
- [7] MetalPrices.com, July 2015. [Online]. Available: <http://www.metalprices.com/metal/copper/cme-future-copper-gc1!>, <http://www.metalprices.com/metal/copper/cme-future-copper-sil1!>, <http://www.metalprices.com/metal/copper/cme-future-copper-hg1!>. [Accessed 23 July 2015].
- [8] A. F. Holleman and N. Wiberg, *Inorganic Chemistry*, San Diego: Academic Press, 2001.

- [9] G. L. Trigg and E. H. Immergut, "4: Combustion to Diamagnetism," in Encyclopedia of Applied Physics, Wiley - VCH , 1992, pp. 267 - 272.
- [10] G. J. Russ, "Electrical Characteristics of Contacts Contaminated With Silver Sulfide Film," IEEE Transactions on Parts, Materials, and Packaging, vol. 6, pp. 129 - 137, 1970.
- [11] P. H. Buffat, "Size Effect on the Melting Temperature of Gold Particles," Phys Rev A, vol. 13, no. 6, pp. 2287-2298, 1976.
- [12] K. A. Schroder, S. C. McCool and W. F. Furlan, "Broadcast Photonic Curing of Metallic Nanoparticle Films," in The 2006 NSTI Nanotechnology Conference and Trade Show, 2006.
- [13] A. N. Karabin, Interviewee, Face to Face Discussion of Printmedia. [Interview]. 15 June 2014.
- [14] D. Jang, D. Kim, B. Lee, S. Kim, M. Kang, D. Min and J. Moon, "Nanosized glass frit as an adhesion promoter for ink-jet printed conductive patterns on glass substrates annealed at high temperatures," Journal of Advanced Functional Materials, vol. 18, pp. 2862-2868, 2008.
- [15] Hitachi, Ltd, "News Releases," 26 November 2012. [Online]. Available: <http://www.hitachi.com/New/cnews/121126a.html>. [Accessed 27 July 2015].
- [16] K. Sivaramakrishnan, A. T. Ngo, S. Iyer and T. L. Alford, "Effect of thermal processing on silver thin films of varying thickness deposited on zinc oxide indium tin oxide," Journal of Applied Physics, vol. 105, 2009.
- [17] in Center for the Advancement of Printed Electronics Free Flexible Electronics Networking Event, Kalamazoo, 2014.



- [18] J. West, M. Carter, S. Smith and J. Sears, "Photonic Sintering of Silver Nanoparticles: Comparison of Experiment and Theory," in *Sintering - Methods and Products*, Rijeka, InTech, 2012, pp. 173-188.
- [19] K. J. Lee, B. H. Jun, T. H. Kim and J. Joung, "Direct synthesis and inkjetting of silver nanocrystals toward printed electronics," *Nanotechnology*, vol. 17, pp. 2424-2428, 2006.
- [20] M. J. Guillot, K. A. Schroder and S. C. McCool, "Simulating the Thermal Response of Thin Films During Photonic Curing," in *Proceedings of the ASME 2012 International Mechanical Engineering Congress & Exposition*, Houston, 2012.
- [21] IUPAC. *Compendium of Chemical Terminology (the "Gold Book")*, 2nd ed., Oxford: Blackwell Scientific Publications, 1997.
- [22] G. Bracco and B. Holst, Eds., *Surface Science Techniques*, Berlin: Springer, 2013.
- [23] M. C. Michalski, S. Desobry and J. Hardy, "Food material adhesion: a review.," *Critical Reviews in Food Science and Nutrition*, pp. 591-619, 1997.
- [24] A. Handojo, Y. Zhai, G. Frankel and M. A. Pascall, "Measurement of adhesion strenghts between various milk products on glass surfaces using contact angle measurement an atomic force microscopy," *Journal of Food Engineering*, vol. 92, pp. 305-311, 2009.
- [25] Keithley, "Application Note Series: Measuring the Resistivity and Determining the Conductivity Type of Semiconductor Materials Using a Four-Point Collinear Probe and the Model 6221 DC and AC Current Source," Keithley Instruments, Inc., Cleveland, 2005.
- [26] Hitachi Chemical Co. , *Safety Data Sheet VS-1307*, Katori-Gun, Chiba, 2014.

- [27] Haper Scientific, "QD Proofing System," Harper Scientific, 2015. [Online]. Available: <http://www.harperimage.com/HarperScientific/Phantom-QD/product-25>. [Accessed 1 June 2015].
  
- [28] K. L. Mittal, ""Adhesion Measurement: Recent progress, unsolved problems, and Prospects," Adhesion Measurement of Thin Films, Thick Films, and Bulk Coatings," ASTM, vol. ATSM STP 640, pp. 7-8, 1978.
  
- [29] K. L. Mittal, "Smposium on /adhesion Aspects of Polymeric Coatings," in Proceedings, The /Electrochemical Society, 1981.
  
- [30] S. Mahdi, "Organic/Inorganic Coatings Cured by Ultraviolet Light and Moisture for Automotive Glass," SAE International, vol. 5, no. 2, pp. 499-502, 2012.
  
- [31] N. Chivoranund, S. Jiemsirilers and D. P. Kashima, "Effects of Surface Treatments on Adhesion of Silver Film on Glass Substrate Fabricated by Electroless Plating," Journal of the Australian Ceramic Society, vol. 49, no. 1, pp. 62-69, 2013.
  
- [32] R. L. Hester, "Teaching an Old Standard New Tricks: A new option is available for manufactures using the ASTM D 3359 crosscut adhesion test," SEMicro, 2011. [Online]. Available: [www.adhesivesmag.com](http://www.adhesivesmag.com).
  
- [33] SEMicro, "Introducing the Permacel P-99 Replacement that's just like the original - only better: The SEMicro CHT line of Cross Hatch Testing Tapes!," The SEMicro CHT line of Cross Hatch Testing Tapes! SEMicro Division, [Online]. Available: <http://www.semicro.org/testtape.aspx>. [Accessed 28 August 2014].
  
- [34] ASTM Standard D 3359-09ε2, "Standard Test Methods for Measuring Adhesion by Tape Test," ASTM International, p. DOI:23, 2009.
  
- [35] Taber Industries, "Taber Abraser 5130/5150," [Online]. Available: [http://www.ccsi-inc.com/taberabraser\\_5130\\_5150.pdf](http://www.ccsi-inc.com/taberabraser_5130_5150.pdf). [Accessed 20 June 2015].

- [36] Abrasion Loss of Paper and Paper Board (Taber Type Method), TAPPI T 476 om11, 2011
  
- [37] D. C. Montgomery, Design and Analysis of Experiments, 8th ed., Hoboken, New Jersey: John Wiley & Sons, Inc, 2013, pp. 80-81.
  
- [38] Minitab Inc., ""Minitab Statistical Glossary", Statistical Significance," 2010.
  
- [39] Minitab Inc, ""Minitab Statistical Glossary," Interaction Plots," 2010.

## APPENDIX

### Analysis of Variance for Experiment 1 and 2

## Factorial Regression: % Film Remaining versus Energy, Adhesion Promoter

### Analysis of Variance

Source	DF	Adj SS	Adj MS	F-Value	P-Value
Model	3	4599.26	1533.09	10.52	0.000
Linear	2	4598.82	2299.41	15.78	0.000
Energy	1	3779.86	3779.86	25.95	0.000
Adhesion Promoter	1	818.96	818.96	5.62	0.024
2-Way Interactions	1	0.44	0.44	0.00	0.956
Energy*Adhesion Promoter	1	0.44	0.44	0.00	0.956
Error	32	4661.62	145.68		
Total	35	9260.88			

### Model Summary

S	R-sq	R-sq(adj)	R-sq(pred)
12.0696	49.66%	44.94%	36.29%

## Factorial Regression: Resistivity (Ohm/sq) versus Energy, Adhesion Promoter

### Analysis of Variance

Source	DF	Adj SS	Adj MS	F-Value	P-Value
Model	3	14.4725	4.8242	153.67	0.000
Linear	2	14.3614	7.1807	228.73	0.000
Energy	1	14.2632	14.2632	454.33	0.000
Adhesion Promoter	1	0.0982	0.0982	3.13	0.087
2-Way Interactions	1	0.1111	0.1111	3.54	0.069
Energy*Adhesion Promoter	1	0.1111	0.1111	3.54	0.069
Error	32	1.0046	0.0314		
Total	35	15.4771			

### Model Summary

S	R-sq	R-sq(adj)	R-sq(pred)
0.177183	93.51%	92.90%	91.78%

## Factorial Regression: % Film Remaining\_2 versus Stage Speed (ft/min), Adhesion Promoter\_2

### Analysis of Variance

Source	DF	Adj SS	Adj MS	F-Value	P-
Value					
Model	3	8428.9	2809.6	25.93	
0.000					
Linear	2	8156.3	4078.2	37.63	
0.000					
Stage Speed (ft/min)	1	8025.4	8025.4	74.06	
0.000					
Adhesion Promoter_2	1	131.0	131.0	1.21	
0.280					
2-Way Interactions	1	272.5	272.5	2.51	
0.123					
Stage Speed (ft/min)*Adhesion Promoter_2	1	272.5	272.5	2.51	
0.123					
Error	32	3467.8	108.4		
Total	35	11896.7			

### Model Summary

S	R-sq	R-sq(adj)	R-sq(pred)
10.4100	70.85%	68.12%	63.11%

## Factorial Regression: Resistivity (Ohm versus Stage Speed (ft/, Adhesion Promote

### Analysis of Variance

Source	DF	Adj SS	Adj MS	F-Value	P-
Value					
Model	3	5.9878	1.99594	46.58	
0.000					
Linear	2	2.0740	1.03700	24.20	
0.000					
Stage Speed (ft/min)	1	0.3007	0.30067	7.02	
0.012					
Adhesion Promoter_2	1	1.7733	1.77334	41.38	
0.000					
2-Way Interactions	1	3.9138	3.91380	91.33	
0.000					
Stage Speed (ft/min)*Adhesion Promoter_2	1	3.9138	3.91380	91.33	
0.000					
Error	32	1.3713	0.04285		
Total	35	7.3591			

### Model Summary

S	R-sq	R-sq(adj)	R-sq(pred)
0.207007	81.37%	79.62%	76.42%